
Communication-Efficient Heterogeneous Federated Learning with Generalized Heavy-Ball Momentum

Riccardo Zaccone*
Politecnico di Torino
riccardo.zaccone@polito.it

Carlo Masone
Politecnico di Torino
carlo.masone@polito.it

Marco Ciccone
Politecnico di Torino
marco.ciccone@polito.it

Abstract

Federated Learning (FL) has emerged as the state-of-the-art approach for learning from decentralized data in privacy-constrained scenarios. However, system and statistical challenges hinder real-world applications, which demand efficient learning from edge devices and robustness to heterogeneity. Despite significant research efforts, existing approaches (i) are not sufficiently robust, (ii) do not perform well in large-scale scenarios, and (iii) are not communication efficient. In this work, we propose a novel *Generalized Heavy-Ball Momentum* (GHBM), motivating its principled application to counteract the effects of statistical heterogeneity in FL. Then, we present FEDHBM as an adaptive, communication-efficient by-design instance of GHBM. Extensive experimentation on vision and language tasks, in both controlled and realistic large-scale scenarios, provides compelling evidence of substantial and consistent performance gains over the state of the art.²

1 Introduction

The introduction of the Federated Learning (FL) paradigm and FEDAVG algorithm in [26] has sparked significant interest in learning from decentralized data. In FL, a central server orchestrates an iterative two-step training process that involves 1) local training, potentially on a large number of clients, each with its own private data, and 2) the aggregation of these updated local models on the server into a single, shared global model. This process is repeated over several communication rounds. While the inherent privacy-preserving nature of FL is appealing for decentralized applications where data sharing is restricted, it also introduces some challenges. Since local data reflects characteristics of individual clients, limiting the optimization to use only the client’s data can lead to issues caused by *statistical heterogeneity*. This becomes problematic when multiple optimization steps are performed before models are synchronized, causing clients to *drift* away from the ideal global updates [18]. Indeed, heterogeneity has been shown to hinder the convergence of FEDAVG [13], increasing the number of communication rounds to reach a target model quality [30] and impacting final performance.

This problem has received significant attention in recent years, and several algorithms have been proposed to mitigate the effects of heterogeneity. For instance, SCAFFOLD [18] relies on additional control variables to correct the local client’s updates, while FEDDYN uses ADMM to align the global and local client solutions. Other works explored momentum, applied at the server [13] or at client-level to correct local updates [28, 42]. In particular, recently MIME [18, 19] has been proposed

*Corresponding author

²Code is provided for the review process and will be released upon acceptance

as a framework to make local updates mimic that of the centralized method run on i.i.d. data, by employing extra server-level statistics at client side. Albeit theoretically grounded, these methods are not sufficiently robust to handle cases of extreme heterogeneity or large-scale problems. Indeed, such problems are known for the case of FEDDYN [1] and SCAFFOLD [18] as found in [36, 30].

In this paper we find that, while motivated by the intuition of integrating the global direction into client updates, prior works using momentum [42, 28, 19] also present failure cases, especially in real-world large-scale scenarios. Furthermore, the current approaches usually imply increased communication for exchanging the additional information needed to correct local updates [18, 19], and so may be unsuitable in a regimen of limited communication resources. These aspects constitute an important factor that hinders the adoption of FL algorithms for real-world cases and motivates the research of more robust, effective, and efficient algorithms pursued in this work.

We attribute the issues of client-level momentum methods to the partial participation and heterogeneity of local datasets, which worsen the estimate of the averaged gradient used by the server when updating the model. Since momentum is a moving average of that gradient, also its estimate is affected. Therefore, methods relying on the classical momentum formulation fail to yield an effective correction. To address these challenges, we propose FEDHBM, a FL algorithm based on a novel *Generalized Heavy-Ball* (GHBM) formulation of momentum that consists of calculating it as a decayed average of τ past momentum terms. In adopting this approach, we demonstrate that our solution effectively incorporates information from the gradients of other clients into the local momentum. This results in a more consistent correction towards the global direction, leading to significantly improved performance.

Contributions. We summarize our main results below.

- We present a novel formulation of momentum called *Generalized Heavy-Ball* (GHBM) momentum, which extends the classical heavy-ball [29], and propose its principled application in FL to counteract the effects of statistical heterogeneity.
- Based on the GHBM principle, we introduce FEDHBM, a new federated optimization algorithm that is robust to heterogeneity and communication-efficient by design.
- We empirically show that existing FL algorithms suffer severe limitations in extreme non-iid scenarios and real-world settings. In contrast, FEDHBM is extremely robust and achieves higher model quality with significantly faster convergence speeds than other client-drift correction methods.

2 Related works

The problem of statistical heterogeneity. The detrimental effects of non-iid data in FL were first observed by [45], who proposed mitigating performance loss by broadcasting a small portion of public data to reduce the divergence between clients' distributions. Alternatively, [22] uses server-side public data for knowledge distillation. Both approaches rely on the strong assumption of readily available and suitable data. Recognizing weight divergence as a source of performance loss FEDPROX [24] adds a regularization term to penalize divergence from the global model. Nevertheless, this was proved ineffective in addressing data heterogeneity [4]. Other works [21, 43, 44, 3] explored grouping clients based on their data distribution to mitigate the challenges of aggregating divergent models.

Stochastic Variance Reduction in FL. Stochastic variance reduction techniques have been applied in FL [6, 23] with SCAFFOLD [18] providing for the first time convergence guarantees for arbitrarily heterogeneous data. The authors also shed light on the *client-drift* of local optimization, which results in slow and unstable convergence. SCAFFOLD uses control variates to estimate the direction of the server model and clients' models and to correct the local update. This approach requires double the communication to exchange the control variates, and it is not robust enough to handle large-scale scenarios akin to cross-device FL [30, 19]. Conversely, we use a novel formulation of momentum that allows gracefully decay of old and stale gradients while achieving robustness to extreme heterogeneity and low participation and propose an algorithm that does not require any additional data exchange.

ADMM and adaptivity. Other methods are based on the Alternating Direction Method of Multipliers [7, 10, 37]. In particular, FEDDYN[1] dynamically modifies the loss function such that the model parameters converge to stationary points of the global empirical loss. Although technically it enjoys the same convergence properties of SCAFFOLD without suffering from its increased communication cost, in practical cases it has displayed problems in dealing with pathological non-iid settings [36].

Other works explored the use of adaptivity to speed up the convergence of FedAvg and reduce the communication overhead [41, 30].

Use of momentum as local correction. As a first attempt, Hsu et al. [13] adopted momentum at server-side to reduce the impact of heterogeneity. However, it has been proven of limited effectiveness under high heterogeneity, because the drift happens at the client level. This motivated later approaches that apply server momentum at each local step [28, 42], and the more general approach by Karimireddy et al. [19] to adapt any centralized optimizer to cross-device FL. It employs a combination of control variates and server optimizer state (*e.g.* momentum) at each client step, which lead to increased communication bandwidth and frequency. A recent similar approach [8] employs compressed updates, still requiring significantly more computation client-side. Rather differently from previous works, FEDHBM is based on our novel *Generalized Heavy-Ball Momentum* (GHBM): it consists in a decayed average of the previous τ momentum terms instead of considering only the last one, and it is designed to more steadily incorporate the descent information of clients selected at past rounds, to be used into local steps as client drift correction. Indeed, the classical heavy-ball [29] is a special case of GHBM. Remarkably, we show our formulation is crucial to effectively counteract the effects of statistical heterogeneity, and yet it is communication efficient by design.

Lowering communication requirements in FL. Researchers have studied methods to reduce the memory needed for exchanging gradients in the distributed setting, for example by quantization [2] or by compression [27, 20]. In the context of FL, such ideas have been developed to meet the communication and scalability constraints [31], and to take into account heterogeneity [33]. Our work focuses on the efficient use of the information already being sent in vanilla FEDAVG, so additional techniques to compress that information remain orthogonal to our approach.

3 Method

3.1 Setup

In FL a server and a set \mathcal{S} of clients collaboratively solve a learning problem, with $|\mathcal{S}| = K \in \mathbb{N}^+$. At each round $t \in [T]$, a fraction of $C \in (0, 1]$ clients from \mathcal{S} is selected to participate in the learning process: we denote this portion as $\mathcal{S}^t \subseteq \mathcal{S}$. Each client $i \in \mathcal{S}^t$ receives the server model $\theta_i^{t,0} \equiv \theta^{t-1}$, and performs J_i local optimization steps, using stochastic gradients $\tilde{g}_i^{t,j}$ evaluated on local parameters $\theta_i^{t,j-1}$ and a batch $d_{i,j}$, sampled from its local dataset \mathcal{D}_i . Similarly, we denote as $g_i^{t,j}$ the corresponding full-batch gradient, *i.e.*, the gradients calculated on all examples of the local dataset. During local training, $\theta_i^{t,j}$ is the model of client i at round t after the j -th optimization step, while $\theta_i^t \equiv \theta^{t,J_i}$ is the model sent back to the server. The server then aggregates the client updates ($\theta^{t-1} - \theta_i^t$), building *pseudo-gradients* [30] that are used to update the model.

3.2 A look back to client drift

One of the core propositions of federated optimization is to take advantage of local work, by running multiple optimization steps on local parameters before synchronization. This has been proven effective for speeding up convergence when local datasets are i.i.d. with respect to a global distribution [35, 25, 26], and it is particularly important for improving communication efficiency, which is the bottleneck when learning in decentralized settings. However, the statistical heterogeneity of clients' local datasets causes local models to *drift* from the ideal trajectory of server parameters, as defined below:

Definition 3.1 (Client drift). Let $\theta_i^{t,j}$, with $j \in [1, J]$ the sequence of local models obtained by local training of client i in an FL algorithm. Define $\theta^{t,j} := \theta^{t,j-1} - \frac{1}{|\mathcal{S}|} \sum_{i=1}^{|\mathcal{S}|} g_i^{t,j}(\theta^{t,j-1})$ as a *shadow sequence* of global models, obtained as if clients' gradients were averaged after each local step [38]. We define the *client-drift* as:

$$\varepsilon_t := \frac{1}{|\mathcal{S}|J} \sum_{i=1}^{|\mathcal{S}|} \sum_{j=1}^J \mathbb{E} \left[\left\| \theta_i^{t,j} - \theta^{t,j} \right\|^2 \right] \quad (1)$$

Main idea. Our way of approaching the problem stems from the intuition that, if at each step the information on the global trajectory would be available, it could be used as a correction to mitigate the divergence with respect to the ideal global update. A way to integrate the descent direction of

past rounds into local updates is by using momentum. However, as revealed by our experimentation, using classical momentum into local updates as implemented by prior works [42, 28, 19] is often not robust enough to provide an effective correction in extreme non-iid scenarios, or when faced with more complex tasks (see Sec. 5). This motivates the introduction of a new form of momentum, that provides a more effective correction to the local training, as explained in the following section.

3.3 Generalized Heavy-Ball Momentum (GHBM)

To overcome the limitations of classical momentum in FL, we propose a novel generalized formulation, that we call *Generalized Heavy-Ball Momentum* (GHBM). Classical momentum consists of a moving average of past gradients, and it is commonly expressed as in eq. (2), which can be equivalently expressed in a version commonly referred to as *heavy-ball momentum* in eq. (3) (see lemma B.1):

HEAVY-BALL MOMENTUM (HBM)

$$\begin{aligned} \tilde{m}^t &\leftarrow \beta \tilde{m}^{t-1} + \tilde{g}^t(\theta^{t-1}) & (2) \quad \tilde{m}^t &\leftarrow (\theta^{t-1} - \theta^{t-2}) & (3) \\ \theta^t &\leftarrow \theta^{t-1} - \eta \tilde{m}^t & & \theta^t &\leftarrow \theta^{t-1} - \eta \tilde{g}^t(\theta^{t-1}) + \beta \tilde{m}^t \end{aligned}$$

Instead, our proposed formulation consists of calculating the momentum term as the decayed average of past τ momentum terms. In practice, at each time step t , the updated momentum term \tilde{m}_τ^t is calculated as in eq. (4), which can still be expressed in a heavy-ball form as in 5. This translates into considering a delta $\tau > 1$ between the two terms (see lemma B.2):

GENERALIZED HEAVY-BALL MOMENTUM (GHBM)

$$\begin{aligned} \tilde{m}_\tau^t &\leftarrow \frac{1}{\tau} \sum_{k=1}^{\tau} \beta \tilde{m}_\tau^{t-k} + \tilde{g}^t(\theta^{t-1}) & (4) \quad \tilde{m}_\tau^t &\leftarrow \frac{1}{\tau} (\theta^{t-1} - \theta^{t-\tau-1}) & (5) \\ \theta^t &\leftarrow \theta^{t-1} - \eta \tilde{m}_\tau^t & & \theta^t &\leftarrow \theta^{t-1} - \eta \tilde{g}^t(\theta^{t-1}) + \beta \tilde{m}_\tau^t \end{aligned}$$

As it is trivial to notice, GHBM with $\tau = 1$ recovers the classical momentum, which existing momentum FL algorithms are based on [42, 28].

3.4 GHBM for client drift correction in FL

The design choice of controlling $\tau > 1$ is grounded in the fact that in FL partial client participation and heterogeneity of local datasets tend to worsen the estimate of the global gradient. Indeed, the gradient referred to above as \tilde{g}^t in FL is built from updates of clients $i \in \mathcal{S}^t$, which are usually a small portion of all the clients participating in the training. Conversely, our formulation comprises the information of the clients selected in the last τ rounds, allowing a more robust estimate of the momentum. This estimate is then embedded into local updates using the heavy-ball form shown in eq. 5, leading to the following update rule:

$$\text{CLIENT STEP:} \quad \theta_i^{t,j} \leftarrow \theta_i^{t,j-1} - \eta_l \tilde{g}_i^{t,j}(\theta_i^{t,j-1}) + \underbrace{\hat{\beta} (\theta^{t-1} - \theta^{t-\tau-1})}_{\tau\text{-GHBM}} \quad (6)$$

where $\hat{\beta} := \frac{\beta}{\tau J_i}$ is the momentum factor scaled by the number of local steps J_i . The heterogeneity reduction effect achieved by GHBM is then related to the choice of τ , which is considered as an hyperparameter, and it is discussed in Sec. 4.2.

Communication-efficient GHBM From eq. 6, the GHBM algorithm requires the server to additionally send the momentum term (or equivalently $\theta^{t-\tau-1}$) at each round. Since usually it is applied to all model parameters, this introduces a communication overhead of $1.5 \times$ w.r.t. FEDAVG. This additional overhead can actually be avoided if clients participate multiple times in the training process, by letting them store the last model received until the next round they will be selected, and use it to calculate locally the GHBM momentum. More formally, let us denote τ_i as the number of rounds elapsed between two subsequent samplings of client i . Then, from the second time it gets sampled, client i has already the model $\theta^{t-\tau_i-1}$, received at round $t - \tau_i$. We call this version **LOCAL-GHBM**, where τ_i is adaptive and determined stochastically by client participation. This choice for the adaptive value of τ_i , intuitively allows incorporating the gradients of all the clients involved in the training process.

In Sec. 4.2 we show that in a simplified scenario of cyclic client participation (*i.e.* assumption 4.4), $\tau = 1/C$ is the optimal trade-off, and Sec. 5.2 confirm this also holds when clients are uniformly

selected at each round. We empirically found that performance can be further improved by considering $\theta_{i,j}^t$ instead of θ^{t-1} and $\theta_i^{t-\tau_i}$ instead of $\theta^{t-\tau_i-1}$ (see Sec. 5.2). This adds a correction term specific to each client objective, such that it penalizes the direction of the last updates at round $t - \tau_i$ with respect to the progressive updates of local steps at the current round t . The final communication-efficient update rule, named **FEDHBM**, is shown in Algorithm 1.

Algorithm 1: FEDHBM and FedAvg

Require: initial model θ^0 , K clients, C participation ratio, T number of total round, B batch size, η and η_l learning rates.

- 1: **for** $t = 1$ to T **do**
- 2: $\mathcal{S}^t \leftarrow$ subset of clients $\sim \mathcal{U}(\mathcal{S}, \max(1, K \cdot C))$
- 3: **for** $i \in \mathcal{S}^t$ **in parallel do**
- 4: $\theta_i^{t,0} \leftarrow \theta^{t-1}$
- 5: **for** $j = 1$ to J_i **do**
- 6: $m_i^{t,j} \leftarrow (\theta_i^{t,j} - \theta_i^{t-\tau_i})$ **if** $\theta_i^{t-\tau}$ **is set** **else** **0**
- 7: sample a mini-batch $d_{i,j}$ from \mathcal{D}_i
- 8: $\theta_i^{t,j} \leftarrow \theta_i^{t,j-1} - \eta_l \tilde{g}(\theta_i^{t,j-1}, d_{i,j}) + \hat{\beta}_i m_i^{t,j}$
- 9: **end for**
- 10: save locally model θ_i^t
- 11: **end for**
- 12: $\theta^t \leftarrow \theta^{t-1} - \eta \sum_{i \in \mathcal{S}^t} \frac{|\mathcal{D}_i|}{|\mathcal{D}_{\mathcal{S}^t}|} (\theta^{t-1} - \theta_i^t)$
- 13: **end for**

Applicability of GHBM and FEDHBM in FL scenarios. While based on the same principle, our algorithms are suitable for different scenarios. FEDHBM takes advantage of the fact that clients participate multiple times in the training process eliminating the need to send the momentum term from the server. As such, clients are *stateful*, as they require maintaining variables across rounds [17]. On the other hand, GHBM has *stateless* clients, which makes it more suitable for cross-device FL or when additional system challenges prevent clients to store state variables. In Sec. 4.3 we analyze such trade-offs from the perspective of optimization, and in Sec. 5.3 we show that they always perform better than the state-of-art.

4 Theoretical discussion

In this section, we establish the theoretical foundations of our algorithms. Our analysis reveals that: (i) GHBM can approximate the global gradient (lemma 4.5), with τ controlling the trade-off between heterogeneity reduction and estimation error (lemma 4.7); and (ii) the error introduced by considering stochastic gradients at client parameters is controllable, and linearly depends on the variance of gradients and the client drift (lemma 4.6). The proofs are deferred to Appendix B.

4.1 Assumptions

For proving our results we rely on notions of stochastic gradient with bounded variance (4.1) and smoothness of the objective functions of the clients (4.2), common in deep learning.

Assumption 4.1 (Unbiasedness and bounded variance of stochastic gradient).

$$\mathbb{E}_{d_i \sim \mathcal{D}_i} [\tilde{g}_i(\theta, d_i)] = g_i(\theta, \mathcal{D}_i)$$

$$\mathbb{E}_{d_i \sim \mathcal{D}_i} [\|\tilde{g}_i(\theta, d_i) - g_i(\theta, \mathcal{D}_i)\|^2] \leq \sigma^2$$

Assumption 4.2 (Smoothness of client’s objectives). Let it be a constant $L > 0$, then for any i, θ_1, θ_2 the following holds:

$$\|g_i(\theta_1) - g_i(\theta_2)\|^2 \leq L^2 \|\theta_1 - \theta_2\|^2$$

With specific reference to the FL setting, 4.3 provides a formalization of the effect of having heterogeneity of local datasets (*i.e.* $G > 0$). We additionally use another assumption that serves as a simplification for gaining intuition about the role of τ in GHBM for client-drift correction, as it allows us to set apart the stochasticity in client sampling in FL rounds.

Assumption 4.3 (Bounded gradient dissimilarity). There exist a constant $G \geq 0$ such that, $\forall i, \theta$:

$$\frac{1}{|\mathcal{S}|} \sum_{i=1}^{|\mathcal{S}|} \|g_i(\theta) - g(\theta)\|^2 \leq G^2$$

Assumption 4.4 (Cyclic Participation). Let it be \mathcal{S}^t the set of clients participating at any round t . A sampling strategy respecting the following is denoted as “cyclic” with period $\tau = 1/C$:

$$\mathcal{S}^t = \mathcal{S}^{t-\tau} \quad \forall t > \tau \quad \wedge \quad \mathcal{S}^k \cap \mathcal{S}^t = \emptyset \quad \forall k \in (t - \tau, t)$$

4.2 How does GHBM counteract heterogeneity?

Let us recall the intuition provided in Sec. 3.3: the idea was to have a correction term as close as possible to the true gradient w.r.t. the global distribution, to mitigate the drift of clients’ updates. This

translates into the following:

$$\theta_i^{t,j} \leftarrow \theta_i^{t,j-1} - \eta \left(g_i^{t,j}(\theta_i^{t,j-1}) + g^t(\theta^{t-1}) \right) \quad (7)$$

Up to the gradient $g^t := \frac{1}{|\mathcal{S}|} \sum_{i=1}^{|\mathcal{S}|} g_i^t$ getting stale along the multiple optimization steps, the above update rule provides effective client-drift correction, as local updates share a common direction. To provide insight about why GHBM is a better choice in the tackled heterogeneous FL scenario, we aim to answer the following three questions.

Question 1. *How well does GHBM with parameter τ approximate the gradient of clients selected in the last τ rounds?*

Let us consider an approximation of g^t , which consists of the averaged gradients of the clients selected in the last τ rounds, that is $\mathcal{S}_\tau^t := \cup_{k=0}^{\tau-1} \mathcal{S}^{t-k}$ and $g^{t_\tau} = \frac{1}{|\mathcal{S}_\tau^t|} \sum_{i=1}^{|\mathcal{S}_\tau^t|} g_i^t$. However, since requiring all the clients to participate in each round violates the premises of FL, g^{t_τ} can only be constructed from gradients taken at parameters of different rounds. Nevertheless, the momentum term \tilde{m}_τ^t has a deviation from $g^{(t-1)_\tau}$ bounded by the following lemma:

Lemma 4.5 (Deviation of τ -GHB momentum from τ -averaged gradients). *Under assumptions 4.1-4.2, it holds that:*

$$\mathbb{E} \left[\left\| \frac{1}{(1 + \hat{\beta})^\tau - 1} \sum_{k=t-\tau}^{t-1} \hat{\beta}(1 + \hat{\beta})^{t-k-1} g^k - g^{(t-1)_\tau} \right\|^2 \right] \leq L^2(\tau - 1) \sum_{k=t-\tau}^{t-2} \mathbb{E} \left[\|\theta^{k+1} - \theta^k\|^2 \right]$$

Question 2. *Since the momentum term in GHBM is built from server-aggregated client gradients, how does this affect its estimate?*

This is indeed one important source of error, and it is shown to affect sensitively the estimate of classical momentum in FL [42, 19]. In fact, server pseudo-gradients $\tilde{g}_i^t := \sum_{j=1}^J \tilde{g}_i^{t,j}(\theta_i^{t,j-1})$ are (i) stochastic (*i.e.*, clients sample mini-batches) and (ii) drifted, that is $\tilde{g}_i^{t,j}$ is taken at intermediate parameters $\theta_i^{t,j-1}$. The following lemma bounds this source of error.

Lemma 4.6 (Variance of τ -GHB momentum). *Under assumptions 4.1-4.2, the update vector m^t in GHB update rule satisfies:*

$$\mathbb{E} \left[\left\| \tilde{m}_\tau^t - \sum_{k=t-\tau}^{t-1} \hat{\beta}(1 + \hat{\beta})^{t-k-1} g^k \right\|^2 \right] \leq \beta J e^{\frac{2\beta}{J}} \left(L^2 \sum_{k=t-\tau}^{t-1} \varepsilon_k + \sigma^2 \right)$$

As it is possible to notice, the error linearly grows with τ , and depends on (i) the noise of stochastic gradients σ^2 and (ii) the client drift ε_t over the past τ rounds. Reasoning on lemma 4.6, assuming the term σ^2 does not dominate, the error due to client drift must also be small for the term on the LHS to remain low. In practical cases (see Section 5.2) we observe remarkable robustness to large values of τ , indicating that a linear dependence on it does not hurt the optimization. The final question regards GHBM's heterogeneity reduction effects.

Question 3. *How does τ impact the effectiveness of GHBM? Intuitively, the best value of τ that minimizes the effect of statistical heterogeneity is the one that allows to comprise a ‘‘snapshot’’ of all clients involved in FL training. The following lemma substantiates this intuition:*

Lemma 4.7 (Deviation of τ -averaged gradient from true gradient). *The approximation of a gradient over the last τ rounds g^{t_τ} w.r.t. the gradient over all clients is quantified by the following:*

$$\mathbb{E} \left[\|g^{t_\tau} - g^t\|^2 \right] \leq 8 \mathbb{E} \left[\left(\frac{|\mathcal{S}| - |\mathcal{S}_\tau^t|}{|\mathcal{S}|} \right)^2 \right] \left(G^2 + \|g^t\|^2 \right)$$

While in this work we assume clients are uniformly sampled without replacement at each round and perform the experiments accordingly, to provide a guideline on how to set τ in practice, in theory, we simplify the problem of client sampling by adopting assumption 4.4 to state the following:

Corollary 4.8. Consider lemma 4.7 and further assume that, at each round of FL training, clients are sampled according to a rule satisfying assumption 4.4. Then, for any $\tau \in (0, \frac{1}{C}]$:

$$\|g^{t\tau} - g^t\|^2 \leq 8(1 - \tau C)^2 (G^2 + \|g^t\|^2)$$

In practice, under the simplified scenario of assumption 4.8, the choice of $\tau = 1/C$ minimizes both the errors in corollary 4.8 and the error introduced in building the momentum term (lemma 4.6). Setting $\tau > 1/C$ intuitively should not provide additional advantages, as the momentum term already comprises the gradients of all clients. Outside the ideal setting provided by assumption 4.4 we expect a value of $\tau > 1/C$ to achieve a similar effect, but providing a precise estimate is a complex problem³.

4.3 Communication efficiency and tradeoffs

In FL, *communication efficiency* refers to the exchange of model and auxiliary parameters between clients and the server [40]. FEDHBM is efficient in the light of data heterogeneity, because (i) it converges in fewer rounds and (ii) does not require sending more data per round. However, in settings with extremely low client participation, FEDHBM will likely be sub-optimal, because the adaptive τ will be too high: indeed the choice of τ comes from a trade-off between heterogeneity reduction effect and introduced bias. In such cases GHBM is the algorithm of choice, as τ can be controlled by the server: the practical implications are discussed in Sec. 5.3, where it is proved that even in this case our solutions improve the state-of-art by a large margin. In practice, our algorithms are flexible to a broad set of scenarios, leaving the choice of the algorithm to the constraint of the specific application.

5 Experimental Results

We present evidence both in controlled and real-world scenarios, showing that: (i) the GHBM formulation is pivotal to enable momentum to provide an effective correction even in extreme heterogeneity, (ii) our adaptive LOCAL-GHBM effectively exploits client participation to enhance communication efficiency and (iii) our proposed algorithms are suitable for cross-device scenarios, with stark improvement on large datasets and architectures (e.g. ViT-B\16).

5.1 Setup

Scenarios, Datasets and Models. For the controlled scenarios, we employ CIFAR-10/100 as computer vision tasks, with RESNET-20 and the same CNN similar to a LeNet-5 commonly used in FL works [14], and SHAKESPEARE dataset as NLP task following [30, 19]. For CIFAR-10/100, the local datasets are obtained by sampling the examples according to a Dirichlet distribution with concentration parameter α , as is common practice [14] (additional details in Appendix C.2). We denote as NON-IID and IID respectively the splits corresponding to $\alpha = 0$ and $\alpha = 10.000$, while for SHAKESPEARE we use instead the predefined splits [5]. The datasets are partitioned among $K = 100$ clients, selecting a portion $C = 10\%$ of them at each round.

As real-world scenarios, we adopt the large-scale GLDV2 and INATURALIST datasets as CV tasks, with both a ViT-B\16 [9] and a MOBILENETV2 [32] pretrained on ImageNet, and STACKOVERFLOW dataset as NLP task, following [30, 19]. These settings are particularly challenging, because the learning tasks are complex, the number of client is high and the client participation (for convenience directly reported in Tab. 2) is scarce (see Appendix C.1 for details).

Metrics and Experimental protocol. As metrics, we consider *final model quality*, as the top-1 accuracy over the last 100 rounds of training (Tab. 1-2, Fig. 4), and *communication/computational efficiency*: this is evaluated by measuring the amount of exchanged bytes and the wall-clock time spent by an algorithm to reach the performance of FEDAVG (Tab. 3). These two metrics together provide a comprehensive evaluation of a FL algorithm for practical scenarios. Results are always reported as the average over 5 independent runs, performed on the best-performing hyperparameters extensively and carefully searched separately for all competitor algorithms. For additional details about the datasets, splits, model architectures, and algorithms’ hyperparameters, see Appendix C.4.

5.2 Counteracting client drift with GHBM

Figure 1 validates our momentum formulation design under worst-case heterogeneity: $\tau > 1$ is crucial to enable momentum to provide an effective correction to client drift. Indeed, previous

³Calculating the number of rounds needed to have sampled each client at least once is an instance of the *Batched Coupons Collector* problem, for which a closed form solution is unknown.

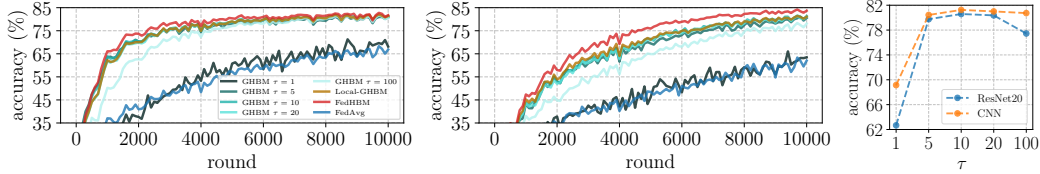


Figure 1: GHBM effectively counteracts the effects of heterogeneity: our momentum formulation ($\tau > 1$) is crucial for superior performance, with an optimal value $\tau = 1/C = 10$, as predicted in theory. Results on CIFAR-10 with CNN (left) and RESNET-20 (right), under worst-case heterogeneity.

momentum-based methods [42, 28], which are special cases of GHBM with $\tau = 1$, are observed to be ineffective in improving FEDAVG. In particular, the best value of τ is experimentally proven to be $\approx 1/C = 10$, as suggested by our theory in Sec. 4.2. Moreover, our approach demonstrates low sensitivity to sub-optimal large values of τ , as both final model quality and convergence speed are only marginally affected (rightmost plot). Interestingly, our communication-efficient instances LOCAL-GHBM and FEDHBM always equal or surpass the best-tuned GHBM, confirming that their adaptive estimate of each client’s momentum positively contributes in a scenario of stochastic client participation, as discussed in Sec. 4.2.

5.3 Comparison with the state-of-art

Results in controlled scenario Our results in Tab. 1 clearly indicate that existing algorithms behave inconsistently when larger models are used (RESNET-20) and fail at improving FEDAVG. In particular, our experimentation reveals that estimating the momentum using full batch gradients as done by MIMEMOM (Karimireddy et al. [19]) does not guarantee an effective correction in most difficult scenarios. Conversely, our algorithms outperform the FEDAVG with an impressive margin of $+20.6\%$ and $+14.4\%$ on RESNET-20 and CNN under worst-case heterogeneity, and consistently over less severe conditions (higher values of α in Fig. 2). We found that testing algorithms on such purposely difficult scenarios adequately renders the expected performance of algorithms when applied to real-world distribution, as our evidence on large-scale settings in the next paragraph suggests.

Table 1: Comparison with state-of-the-art in controlled setting (acc@10k-20k rounds for RESNET-20/CNN). NON-IID ($\alpha = 0$) and IID ($\alpha = 10k$). Best result in **bold**, second best underlined. \times indicates non-convergence.

METHOD	CIFAR-100 (RESNET-20)		CIFAR-100 (CNN)		SHAKESPEARE	
	NON-IID	IID	NON-IID	IID	NON-IID	IID
FEDAVG	21.9±0.9	58.6±0.4	35.6±0.2	49.7±0.2	47.3±0.1	47.1±0.2
FEDPROX	22.1±1.0	58.5±0.3	35.5±0.3	49.9±0.2	47.3±0.1	47.1±0.2
SCAFFOLD	30.7±1.3	58.0±0.6	45.5±0.1	49.4±0.4	50.2±0.1	50.1±0.1
FEDDYN	6.0±0.5	60.8±0.7	\times	51.9±0.2	50.7±0.2	50.8±0.2
ADABEST	8.4±2.0	55.6±0.3	35.6±0.3	49.7±0.2	47.3±0.1	47.1±0.2
MIME	9.0±0.4	59.0±0.3	36.3±0.5	50.9±0.4	48.3±0.2	48.5±0.1
FEDAVGM	22.8±0.8	58.7±0.9	35.2±0.3	50.7±0.2	50.0±0.0	50.4±0.1
FEDCM (GHBM $\tau=1$)	22.2±1.0	53.1±0.2	36.0±0.3	50.2±0.5	49.2±0.1	50.4±0.1
FEDADC (GHBM $\tau=1$)	22.4±0.1	53.2±0.2	37.9±0.3	50.2±0.4	49.2±0.1	50.4±0.1
MIMEMOM	21.7±1.1	60.5±0.6	48.2±0.7	50.6±0.1	48.5±0.2	48.9±0.2
MIMELITEMOM	14.4±0.6	59.2±0.5	46.0±0.3	50.7±0.1	49.1±0.4	49.4±0.3
LOCAL-GHBM (ours)	38.2±1.0	62.0±0.5	50.3±0.5	51.9±0.4	51.2±0.1	51.1±0.3
FEDHBM (ours)	42.5±0.8	62.5±0.5	50.4±0.5	52.0±0.4	51.3±0.1	51.4±0.2

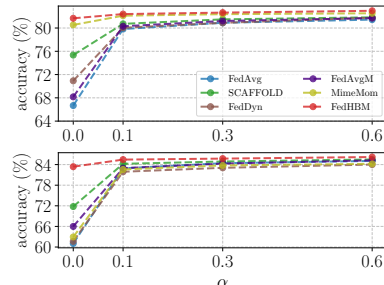


Figure 2: Final model quality at different values of α (lower $\alpha \rightarrow$ higher heterogeneity) on CIFAR-10, with CNN (top) and RESNET-20 (bottom).

Results in real-world large-scale scenarios Extending the experimentation to settings characterized by extremely low client participation, we test both our GHBM with τ tuned via a grid-search and our adaptive FEDHBM, which exploits client participation to keep the same communication complexity of FEDAVG. As discussed in Sec. 4.3, under such extreme client participation patterns GHBM performs better because the trade-off between heterogeneity reduction and bias is explicitly tuned by the choice of the best performing τ , while FEDHBM will likely adopt a suboptimal value. However, results in Tab. 2 show a stark improvement over the state-of-art for both our algorithms, indicating that the design principle of our momentum formulation is remarkably robust and provides effective improvement even when client participation is very low ($e.g. C \leq 1\%$).

Communication efficiency To demonstrate the communication-efficiency of our algorithms, in Tab. 3 we calculated the communication and computational cost of our simulations for reaching the performance of FEDAVG (details on the procedure in Appendix C.3). These analyses reveal that our proposed algorithms lead to a dramatic reduction in both communication and computational cost,

Table 2: Test accuracy (%) comparison of best SOTA FL algorithms on large-scale and realistic settings. GHBM is the best algorithm when client participation is extremely low, while FEDHBM still improves the other competitors by a large margin. ✗ means that the algorithm did not converge.

METHOD	MOBILENETV2				ViT-B/16			STACKOVERFLOW
	GLDV2	INATURALIST			GLDV2	INATURALIST		
	$C \approx 0.79\%$	$C \approx 0.1\%$	$C \approx 0.5\%$	$C \approx 1\%$	$C \approx 0.79\%$	$C \approx 0.1\%$	$C \approx 0.5\%$	
FEDAVG	60.3 ± 0.2	38.0 ± 0.8	45.25 ± 0.1	47.59 ± 0.1	68.5 ± 0.5	65.6 ± 0.1	70.7 ± 0.8	24.0 ± 0.4
SCAFFOLD	61.0 ± 0.1	✗	✗	✗	67.5 ± 3.3	✗	✗	24.8 ± 0.4
FEDAVGM	61.5 ± 0.2	41.3 ± 0.4	46.0 ± 0.1	48.4 ± 0.1	70.0 ± 0.5	66.0 ± 0.2	71.4 ± 0.5	24.1 ± 0.3
MIMEMOM	✗	✗	✗	✗	✗	✗	✗	24.9 ± 0.6
GHBM - best τ (ours)	65.9 ± 0.1	41.8 ± 0.1	48.7 ± 0.1	50.5 ± 0.1	74.3 ± 0.6	68.8 ± 0.3	73.5 ± 0.4	27.0 ± 0.1
FEDHBM (ours)	65.4 ± 0.2	41.6 ± 0.2	47.3 ± 0.0	49.8 ± 0.0	73.1 ± 0.9	66.7 ± 0.7	72.1 ± 0.5	24.5 ± 0.4

with an average saving of respectively +67.5% and +62.5%. In practice, both our algorithms show faster convergence and higher final model quality: in particular, in settings with extremely low client participation (e.g. GLDV2 and INATURALIST), GHBM is more suitable for best accuracy, while FEDHBM is the best at lowering the communication cost.

Table 3: Communication and computational cost of the SOTA FL algorithms for reaching the final model quality of FEDAVG, across academic and real-world large-scale datasets (details on how this table is made can be found in Appendix C.3). The coloured arrows indicate respectively a reduction (↓) and an increase (↑) of communication/computational cost.

METHOD	COMM. OVERHEAD	COMMUNICATION COST (BYTES EXCHANGED)				COMPUTATIONAL COST (WALL-CLOCK TIME HH:MM)			
		CIFAR-100 ($\alpha = 0$)		GLDV2		CIFAR-100 ($\alpha = 0$)		GLDV2	
		CNN	RESNET-20	MOBILENETV2	ViT-B/16	CNN	RESNET-20	MOBILENETV2	ViT-B/16
FEDAVG	1×	30.9 GB	10.3 GB	89.8 GB	483.7 GB	02:05	03:36	13:51	13:56
SCAFFOLD	2×	31.8 GB ↑ 3.0%	12.1 GB ↑ 17.5%	51.2 GB ↓ 43.0%	967.4 GB ↑ 100.0%	01:15 ↓ 40.0%	02:27 ↓ 41.0%	08:28 ↓ 38.9%	15:15 ↑ 9.4%
FEDAVGM	1×	28.9 GB ↓ 6.5%	9.2 GB ↓ 10.7%	73.6 GB ↓ 18.0%	403.1 GB ↓ 16.7%	01:57 ↓ 6.5%	03:14 ↓ 10.2%	11:22 ↓ 18.0%	11:37 ↓ 16.7%
MIMEMOM	3×	21.5 GB ↓ 30.4%	30.9 GB ↑ 200.0%	269.4 GB ↑ 200.0%	1.417 TB ↑ 200.0%	01:27 ↓ 30.4%	10:42 ↑ 197.8%	41:07 ↑ 197.8%	41:30 ↑ 197.8%
GHBM (ours)	1.5×	6.4 GB ↓ 79.3%	6.3 GB ↓ 38.8%	48.5 GB ↓ 46.0%	314.4 GB ↓ 35.0%	00:19 ↓ 84.2%	01:28 ↓ 59.3%	05:20 ↓ 61.5%	06:30 ↓ 53.3%
FEDHBM (ours)	1×	3.9 GB ↓ 87.4%	3.7 GB ↓ 64.1%	29.6 GB ↓ 67.0%	234.4 GB ↓ 51.5%	00:17 ↓ 86.0%	01:18 ↓ 63.9%	06:23 ↓ 54.0%	07:31 ↓ 46.0%

5.4 Notes on failure cases of SOTA algorithms

In this paper, we evaluated our approach using the large-scale FL datasets proposed by [14]. Notably, several recent state-of-the-art FL algorithms failed to converge on these datasets. For SCAFFOLD this result aligns with prior works [30, 19], since it is unsuitable for cross-device FL with thousands of devices. Indeed, the client control variates can become stale, and may consequently degrade the performance. For MIMEMOM [19], despite extensive hyperparameter tuning using the authors’ original code, we were unable to achieve convergence. This finding is surprising since the approach has been proposed to tackle cross-device FL. To our knowledge, this is the first work to report these failure cases, likely due to the lack of prior evaluations on such challenging datasets. We believe these findings underscore the need for further investigation into the factors contributing to algorithm performance in large-scale, heterogeneous FL settings.

6 Broader Impact and Limitations

The algorithms presented in this work offer a substantial advancement in federated training efficiency. By significantly improving performance while reducing computational, communication, and energy costs, our approach contributes to a more sustainable and scalable federated learning ecosystem. This marks a notable step towards wider adoption of FL in real-world applications, particularly in the challenging cross-device setting, where our methods have demonstrated remarkable flexibility and effectiveness. Despite these significant improvements over the state-of-the-art, challenges remain in fully realizing the potential of cross-device FL. Our results underscore the critical importance of accurately estimating the global direction for rapid algorithm convergence. Both GHBM and FEDHBM leverage this insight, correcting client drift through global direction estimation. However, the accurate estimation of this direction in extremely large-scale scenarios (e.g., millions of clients with low participation rates) remains an open research problem.

7 Conclusions

In this work, we propose a novel *Generalized Heavy-Ball Momentum* (GHBM), motivating its principled application in FL to counteract the effects of statistical heterogeneity. Based on GHBM, we present FEDHBM as an adaptive instance which is additionally communication-efficient by design. Our results in large-scale scenarios largely improve the state of art both in final model quality and communication efficiency. The generality and versatility of the novel GHBM formulation expands its potential applications to a wider range of scenarios where communication is a bottleneck, such as distributed learning.

References

- [1] Durmus Alp Emre Acar, Yue Zhao, Ramon Matas Navarro, Matthew Mattina, Paul N Whatmough, and Venkatesh Saligrama. Federated learning based on dynamic regularization. *International Conference on Learning Representations*, 2021.
- [2] Dan Alistarh, Demjan Grubic, Jerry Li, Ryota Tomioka, and Milan Vojnovic. Qsgd: Communication-efficient sgd via gradient quantization and encoding. In I. Guyon, U. Von Luxburg, S. Bengio, H. Wallach, R. Fergus, S. Vishwanathan, and R. Garnett, editors, *Advances in Neural Information Processing Systems*, volume 30. Curran Associates, Inc., 2017. URL https://proceedings.neurips.cc/paper_files/paper/2017/file/6c340f25839e6acdc73414517203f5f0-Paper.pdf.
- [3] Debora Caldarola, Massimiliano Mancini, Fabio Galasso, Marco Ciccone, Emanuele Rodola, and Barbara Caputo. Cluster-driven graph federated learning over multiple domains. In *Proceedings of the IEEE/CVF Conference on Computer Vision and Pattern Recognition (CVPR) Workshops*, pages 2749–2758, June 2021.
- [4] Debora Caldarola, Barbara Caputo, and Marco Ciccone. Improving generalization in federated learning by seeking flat minima. In *Computer Vision—ECCV 2022: 17th European Conference, Tel Aviv, Israel, October 23–27, 2022, Proceedings, Part XXIII*, pages 654–672. Springer, 2022.
- [5] Sebastian Caldas, Sai Meher Karthik Duddu, Peter Wu, Tian Li, Jakub Konečný, H. Brendan McMahan, Virginia Smith, and Ameet Talwalkar. Leaf: A benchmark for federated settings, 2019.
- [6] Dawei Chen, Choong Seon Hong, Yiyong Zha, Yunfei Zhang, Xin Liu, and Zhu Han. Fedsvrg based communication efficient scheme for federated learning in mec networks. *IEEE Transactions on Vehicular Technology*, 70(7):7300–7304, 2021. doi: 10.1109/TVT.2021.3089431.
- [7] Yicheng Chen, Rick S. Blum, and Brian M. Sadler. Communication efficient federated learning via ordered admm in a fully decentralized setting. In *2022 56th Annual Conference on Information Sciences and Systems (CISS)*, pages 96–100, 2022. doi: 10.1109/CISS53076.2022.9751166.
- [8] Rudrajit Das, Anish Acharya, Abolfazl Hashemi, sujay sanghavi, Inderjit S Dhillon, and ufuk topcu. Faster non-convex federated learning via global and local momentum. In *The 38th Conference on Uncertainty in Artificial Intelligence*, 2022. URL <https://openreview.net/forum?id=SS1LRUIs9e9>.
- [9] Alexey Dosovitskiy, Lucas Beyer, Alexander Kolesnikov, Dirk Weissenborn, Xiaohua Zhai, Thomas Unterthiner, Mostafa Dehghani, Matthias Minderer, Georg Heigold, Sylvain Gelly, Jakob Uszkoreit, and Neil Houlsby. An image is worth 16x16 words: Transformers for image recognition at scale. In *International Conference on Learning Representations*, 2021. URL <https://openreview.net/forum?id=YicbFdNTTy>.
- [10] Yonghai Gong, Yichuan Li, and Nikolaos M. Freris. Fedadmm: A robust federated deep learning framework with adaptivity to system heterogeneity, 2022.
- [11] Kaiming He, Xiangyu Zhang, Shaoqing Ren, and Jian Sun. Deep residual learning for image recognition, 2015.
- [12] Kevin Hsieh, Amar Phanishayee, Onur Mutlu, and Phillip Gibbons. The non-IID data quagmire of decentralized machine learning. In Hal Daumé III and Aarti Singh, editors, *Proceedings of the 37th International Conference on Machine Learning*, volume 119 of *Proceedings of Machine Learning Research*, pages 4387–4398. PMLR, 13–18 Jul 2020. URL <https://proceedings.mlr.press/v119/hsieh20a.html>.
- [13] Tzu-Ming Harry Hsu, Hang Qi, and Matthew Brown. Measuring the effects of non-identical data distribution for federated visual classification, 2019.

- [14] Tzu-Ming Harry Hsu, Hang Qi, and Matthew Brown. Federated visual classification with real-world data distribution. In Andrea Vedaldi, Horst Bischof, Thomas Brox, and Jan-Michael Frahm, editors, *Computer Vision – ECCV 2020*, pages 76–92, Cham, 2020. Springer International Publishing. ISBN 978-3-030-58607-2.
- [15] Yerlan Idelbayev. Proper ResNet implementation for CIFAR10/CIFAR100 in PyTorch. https://github.com/akamaster/pytorch_resnet_cifar10. Accessed: 2023-04-12.
- [16] Sergey Ioffe and Christian Szegedy. Batch normalization: Accelerating deep network training by reducing internal covariate shift. In *International conference on machine learning*, pages 448–456. pmlr, 2015.
- [17] Peter Kairouz, H. Brendan McMahan, Brendan Avent, Aurélien Bellet, Mehdi Bennis, Arjun Nitin Bhagoji, Kallista Bonawitz, Zachary Charles, Graham Cormode, Rachel Cummings, Rafael G. L. D’Oliveira, Hubert Eichner, Salim El Rouayheb, David Evans, Josh Gardner, Zachary Garrett, Adrià Gascón, Badih Ghazi, Phillip B. Gibbons, Marco Gruteser, Zaid Harchaoui, Chaoyang He, Lie He, Zhouyuan Huo, Ben Hutchinson, Justin Hsu, Martin Jaggi, Tara Javidi, Gauri Joshi, Mikhail Khodak, Jakub Konečný, Aleksandra Korolova, Farinaz Koushanfar, Sanmi Koyejo, Tancrede Lepoint, Yang Liu, Prateek Mittal, Mehryar Mohri, Richard Nock, Ayfer Özgür, Rasmus Pagh, Hang Qi, Daniel Ramage, Ramesh Raskar, Mariana Raykova, Dawn Song, Weikang Song, Sebastian U. Stich, Ziteng Sun, Ananda Theertha Suresh, Florian Tramèr, Praneeth Vepakomma, Jianyu Wang, Li Xiong, Zheng Xu, Qiang Yang, Felix X. Yu, Han Yu, and Sen Zhao. Advances and open problems in federated learning. *Found. Trends Mach. Learn.*, 14 (1–2):1–210, jun 2021. ISSN 1935-8237. doi: 10.1561/22000000083. URL <https://doi.org/10.1561/22000000083>.
- [18] Sai Praneeth Karimireddy, Satyen Kale, Mehryar Mohri, Sashank Reddi, Sebastian Stich, and Ananda Theertha Suresh. Scaffold: Stochastic controlled averaging for federated learning. In *International Conference on Machine Learning*, pages 5132–5143. PMLR, 2020.
- [19] Sai Praneeth Karimireddy, Martin Jaggi, Satyen Kale, Mehryar Mohri, Sashank J. Reddi, Sebastian U Stich, and Ananda Theertha Suresh. Breaking the centralized barrier for cross-device federated learning. In A. Beygelzimer, Y. Dauphin, P. Liang, and J. Wortman Vaughan, editors, *Advances in Neural Information Processing Systems*, 2021. URL <https://openreview.net/forum?id=FMPuzXV1fR>.
- [20] Anastasia Koloskova*, Tao Lin*, Sebastian U Stich, and Martin Jaggi. Decentralized deep learning with arbitrary communication compression. In *International Conference on Learning Representations*, 2020. URL <https://openreview.net/forum?id=SkgGCKrKvH>.
- [21] Kavya Kopparapu and Eric Lin. Fedfmc: Sequential efficient federated learning on non-iid data. *arXiv preprint arXiv:2006.10937*, 2020.
- [22] Daliang Li and Junpu Wang. Fedmd: Heterogenous federated learning via model distillation. *arXiv preprint arXiv:1910.03581*, 2019.
- [23] Tian Li, Anit Kumar Sahu, Manzil Zaheer, Maziar Sanjabi, Ameet Talwalkar, and Virginia Smith. Feddane: A federated newton-type method. *2019 53rd Asilomar Conference on Signals, Systems, and Computers*, pages 1227–1231, 2019.
- [24] Tian Li, Anit Kumar Sahu, Manzil Zaheer, Maziar Sanjabi, Ameet Talwalkar, and Virginia Smith. Federated optimization in heterogeneous networks. *Proceedings of Machine Learning and Systems*, 2:429–450, 2020.
- [25] Tao Lin, Sebastian U. Stich, Kumar Kshitij Patel, and Martin Jaggi. Don’t use large mini-batches, use local sgd. In *International Conference on Learning Representations*, 2020. URL <https://openreview.net/forum?id=B1ey01BFPr>.
- [26] Brendan McMahan, Eider Moore, Daniel Ramage, Seth Hampson, and Blaise Aguera y Arcas. Communication-efficient learning of deep networks from decentralized data. In *Artificial intelligence and statistics*, pages 1273–1282. PMLR, 2017.
- [27] Konstantin Mishchenko, Eduard Gorbunov, Martin Takáč, and Peter Richtárik. Distributed learning with compressed gradient differences, 2019.
- [28] Emre Ozfatura, Kerem Ozfatura, and Deniz Gündüz. Fedadc: Accelerated federated learning with drift control. In *2021 IEEE International Symposium on Information Theory (ISIT)*, pages 467–472. IEEE, 2021. doi: 10.1109/ISIT45174.2021.9517850. URL <http://dx.doi.org/10.1109/ISIT45174.2021.9517850>.
- [29] Boris Polyak. Some methods of speeding up the convergence of iteration methods. *Ussr Computational Mathematics and Mathematical Physics*, 4:1–17, 12 1964. doi: 10.1016/0041-5553(64)90137-5.

- [30] Sashank Reddi, Zachary Charles, Manzil Zaheer, Zachary Garrett, Keith Rush, Jakub Konečný, Sanjiv Kumar, and H Brendan McMahan. Adaptive federated optimization. *International Conference on Learning Representations (ICLR)*, 2021.
- [31] Amirhossein Reisizadeh, Aryan Mokhtari, Hamed Hassani, Ali Jadbabaie, and Ramtin Pedarsani. Fedpaq: A communication-efficient federated learning method with periodic averaging and quantization. In Silvia Chiappa and Roberto Calandra, editors, *Proceedings of the Twenty Third International Conference on Artificial Intelligence and Statistics*, volume 108 of *Proceedings of Machine Learning Research*, pages 2021–2031. PMLR, 26–28 Aug 2020. URL <https://proceedings.mlr.press/v108/reisizadeh20a.html>.
- [32] Mark Sandler, Andrew G. Howard, Menglong Zhu, Andrey Zhmoginov, and Liang-Chieh Chen. Mobilenetv2: Inverted residuals and linear bottlenecks. In *2018 IEEE Conference on Computer Vision and Pattern Recognition, CVPR 2018, Salt Lake City, UT, USA, June 18-22, 2018*, pages 4510–4520. Computer Vision Foundation / IEEE Computer Society, 2018. doi: 10.1109/CVPR.2018.00474. URL http://openaccess.thecvf.com/content_cvpr_2018/html/Sandler_MobileNetV2_Inverted_Residuals_CVPR_2018_paper.html.
- [33] Felix Sattler, Simon Wiedemann, Klaus-Robert Müller, and Wojciech Samek. Robust and communication-efficient federated learning from non-i.i.d. data. *IEEE Transactions on Neural Networks and Learning Systems*, 31(9):3400–3413, 2020. doi: 10.1109/TNNLS.2019.2944481.
- [34] Andreas Peter Steiner, Alexander Kolesnikov, Xiaohua Zhai, Ross Wightman, Jakob Uszkoreit, and Lucas Beyer. How to train your vit? data, augmentation, and regularization in vision transformers. *Transactions on Machine Learning Research*, 2022. ISSN 2835-8856. URL <https://openreview.net/forum?id=4nPswr1KcP>.
- [35] Sebastian U. Stich. Local SGD converges fast and communicates little. In *International Conference on Learning Representations*, 2019. URL <https://openreview.net/forum?id=S1g2JnRcFX>.
- [36] Farshid Varno, Marzie Saghai, Laya Rafiee Sevyeri, Sharut Gupta, Stan Matwin, and Mohammad Havaei. Adabest: Minimizing client drift in federated learning via adaptive bias estimation. In *Computer Vision – ECCV 2022: 17th European Conference, Tel Aviv, Israel, October 23–27, 2022, Proceedings, Part XXIII*, page 710–726, Berlin, Heidelberg, 2022. Springer-Verlag. ISBN 978-3-031-20049-6. doi: 10.1007/978-3-031-20050-2_41. URL https://doi.org/10.1007/978-3-031-20050-2_41.
- [37] Han Wang, Siddhartha Marella, and James Anderson. Fedadmm: A federated primal-dual algorithm allowing partial participation, 2022.
- [38] Jianyu Wang, Zachary Charles, Zheng Xu, Gauri Joshi, H Brendan McMahan, Maruan Al-Shedivat, Galen Andrew, Salman Avestimehr, Katharine Daly, Deepesh Data, et al. A field guide to federated optimization. *arXiv preprint arXiv:2107.06917*, 2021.
- [39] Yuxin Wu and Kaiming He. Group normalization. In *Proceedings of the European Conference on Computer Vision (ECCV)*, September 2018.
- [40] Qi Xia, Winson Ye, Zeyi Tao, Jindi Wu, and Qun Li. A survey of federated learning for edge computing: Research problems and solutions. *High-Confidence Computing*, 1(1):100008, 2021. ISSN 2667-2952. doi: <https://doi.org/10.1016/j.hcc.2021.100008>. URL <https://www.sciencedirect.com/science/article/pii/S266729522100009X>.
- [41] Cong Xie, Oluwasanmi Koyejo, Indranil Gupta, and Haibin Lin. Local adaalter: Communication-efficient stochastic gradient descent with adaptive learning rates. *CoRR*, abs/1911.09030, 2019. URL <http://arxiv.org/abs/1911.09030>.
- [42] Jing Xu, Sen Wang, Liwei Wang, and Andrew Chi-Chih Yao. Fedcm: Federated learning with client-level momentum, 2021.
- [43] Riccardo Zaccone, Andrea Rizzardi, Debora Caldarola, Marco Ciccone, and Barbara Caputo. Speeding up heterogeneous federated learning with sequentially trained superclients. In *2022 26th International Conference on Pattern Recognition (ICPR)*. IEEE, aug 2022. doi: 10.1109/icpr56361.2022.9956084. URL <https://doi.org/10.1109/icpr56361.2022.9956084>.
- [44] Shenglai Zeng, Zonghang Li, Hongfang Yu, Yihong He, Zenglin Xu, Dusit Niyato, and Han Yu. Heterogeneous federated learning via grouped sequential-to-parallel training. In Arnab Bhattacharya, Janice Lee Mong Li, Divyakant Agrawal, P. Krishna Reddy, Mukesh Mohania, Anirban Mondal, Vikram Goyal, and Rage Uday Kiran, editors, *Database Systems for Advanced Applications*, pages 455–471, Cham, 2022. Springer International Publishing. ISBN 978-3-031-00126-0.
- [45] Yue Zhao, Meng Li, Liangzhen Lai, Naveen Suda, Damon Civin, and Vikas Chandra. Federated learning with non-iid data. *arXiv preprint arXiv:1806.00582*, 2018.

A Additional discussion

A.1 Cross-silo and cross-device FL

Setting Cross-silo FL. In this setting, following the characterization in [17], the training nodes are expected to be different organizations or geo-distributed data centers. The number of such nodes is modest ($\mathcal{O}(10^2)$) and they are assumed to be almost always available and reliable. This makes it possible to maintain a state on nodes across two different rounds, and often the use of stateful clients is an indicator for an algorithm to be designed for this scenario. Usually, the problem of FL in such a setting is cast as a finite-sum optimization problem, where each function is the local clients' loss function (eq. 8)

Setting cross-device FL. Differently from cross-silo FL, in the cross-device setting the clients are assumed to be possibly unreliable edge devices, with only a fraction of them available at any given time. As such, communication is the primary bottleneck. Most importantly, they can be massive in number ($\mathcal{O}(10^{10})$), so this motivates the fact that they should be stateless since each client is likely to participate only once in the training procedure. Following the characterization in [19], being the number of clients enormous, this problem can be modeled by introducing the stochasticity client-level, over the possibly sampled clients (eq. 9).

CROSS-SILO:

$$\arg \min_{\theta \in \mathbb{R}^d} \sum_{k \in \mathcal{S}} \frac{|\mathcal{D}_k|}{|\mathcal{D}_S|} \mathbb{E}_{(x,y) \sim \mathcal{D}_k} [L(f_\theta; (x, y))] \quad (8)$$

CROSS-DEVICE:

$$\arg \min_{\theta \in \mathbb{R}^d} \mathbb{E}_{i \sim \mathcal{S}} \left[\sum_{j=1}^{|\mathcal{D}_i|} \frac{1}{|\mathcal{D}_i|} L(f_\theta; (x_j, y_j)) \right] \quad (9)$$

Cross-silo and cross-device in practice. The two aforementioned setups are however extreme cases, and real-world scenarios will likely enjoy some features from both settings. Previous FL works that address cross-silo FL usually experiment with a few hundred devices but account for low participation and unreliability, and treat communication as the primary bottleneck [18, 1]. However, they are stateful, and this has raised concerns about their applicability in cross-device: in particular Karimireddy et al. [19] noticed that the control variates in Karimireddy et al. [18] get stale as clients are not seen again during training, and highlights that stateless clients reflect the different formulation in equations 9, 8. In this work we show that FEDHBM is robust to extremely low participation rates, and that it gets more effective as each client participates in the training process. Remarkably, our method succeeds in scenarios where state-of-art methods fail (see and tables 1-2).

B Proofs

B.1 Momentum expressions

In this section we report the derivation of the momentum expressions in eq. (3) and eq. (5) from the main paper.

Lemma B.1 (Heavy-Ball formulation of classical momentum). *Let us consider the following classical formulation of momentum:*

$$\tilde{m}^t = \beta \tilde{m}^{t-1} + \tilde{g}^t(\theta^{t-1}) \quad (10)$$

$$\theta^t = \theta^{t-1} - \eta \tilde{m}^t \quad (11)$$

The same update rule can be equivalently expressed with the following, known as heavy-ball formulation:

$$\theta^t = \theta^{t-1} + \beta(\theta^{t-1} - \theta^{t-2}) - \eta \tilde{g}(\theta^{t-1}) \quad (12)$$

Proof. First derive the expression of \tilde{m}^t from eq. (11), both for time t and $t - 1$:

$$\tilde{m}^t = \frac{(\theta^{t-1} - \theta^t)}{\eta}$$

$$\tilde{m}^{t-1} = \frac{(\theta^{t-2} - \theta^{t-1})}{\eta}$$

Now plug these expressions into equation (10) to obtain (12):

$$\begin{aligned}\frac{(\theta^{t-1} - \theta^t)}{\eta} &= \beta \frac{(\theta^{t-2} - \theta^{t-1})}{\eta} + \tilde{g}^t(\theta^{t-1}) \\ (\theta^t - \theta^{t-1}) &= \beta (\theta^{t-1} - \theta^{t-2}) - \eta \tilde{g}^t(\theta^{t-1}) \\ \theta^t &= \theta^{t-1} + \beta (\theta^{t-1} - \theta^{t-2}) - \eta \tilde{g}^t(\theta^{t-1})\end{aligned}$$

□

Lemma B.2 (Heavy-Ball formulation of generalized momentum). *Let us consider the following generalized formulation of momentum:*

$$\tilde{m}_\tau^t = \frac{1}{\tau} \sum_{k=1}^{\tau} \beta \tilde{m}_\tau^{t-k} + \tilde{g}^t(\theta^{t-1}) \quad (13)$$

$$\theta^t = \theta^{t-1} - \eta \tilde{m}_\tau^t \quad (14)$$

The same update rule can be equivalently expressed in an heavy ball form, which we call as Generalized Heavy-Ball momentum (GHB):

$$\theta^t = \theta^{t-1} + \frac{\beta}{\tau} (\theta^{t-1} - \theta^{t-\tau-1}) - \eta \tilde{g}^t(\theta^{t-1}) \quad (15)$$

Proof. First derive the expression of \tilde{m}_τ^t from eq. (14), both for time t and $t-1$:

$$\begin{aligned}\tilde{m}_\tau^t &= \frac{(\theta^{t-1} - \theta^t)}{\eta} \\ \tilde{m}_\tau^{t-1} &= \frac{(\theta^{t-2} - \theta^{t-1})}{\eta}\end{aligned}$$

Now plug these expressions into equation (13):

$$\begin{aligned}\frac{(\theta^{t-1} - \theta^t)}{\eta} &= \frac{\beta}{\tau} \sum_{k=1}^{\tau} \frac{(\theta^{t-k-1} - \theta^{t-k})}{\eta} + \tilde{g}^t(\theta^{t-1}) \\ (\theta^t - \theta^{t-1}) &= \frac{\beta}{\tau} \sum_{k=1}^{\tau} (\theta^{t-k} - \theta^{t-k-1}) - \eta \tilde{g}^t(\theta^{t-1}) \\ \theta^t &= \theta^{t-1} + \frac{\beta}{\tau} \sum_{k=1}^{\tau} (\theta^{t-k} - \theta^{t-k-1}) - \eta \tilde{g}^t(\theta^{t-1}) \\ \theta^t &= \theta^{t-1} + \frac{\beta}{\tau} (\theta^{t-1} - \theta^{t-\tau-1}) - \eta \tilde{g}^t(\theta^{t-1})\end{aligned}$$

Where the last equality (15) comes from telescoping the summation on the rhs. □

B.2 Technical lemmas

Now we cover some technical lemmas which are useful for computations later on. These are known results that are reported here for the convenience of the reader.

Lemma B.3 (Recursive moving average). *Let $(c_i)_{i \in \mathbb{N}}$ be a sequence of vectors in \mathbb{R}^d and $b \in \mathbb{R}$ a scalar value. Define the sequence of vectors $(a_i)_{i \in \mathbb{N}}$ such that $a_1 = c_1$ and for any $i > 1$*

$$a_i := \sum_{k=1}^{i-1} b a_k + c_i \quad (16)$$

Then, the following holds

$$a_i = \sum_{k=1}^{i-1} b(1+b)^{i-k-1} c_k + c_i \quad (17)$$

Proof. We proceed by induction. The base step is trivially verified. Now let $i \in \mathbb{N}$ and $i > 1$. Assume that (17) holds for any $k < i$. Then,

$$a_i = \sum_{k=1}^{i-1} ba_k + c_i \quad (18)$$

$$= b \sum_{k=1}^{i-1} \left(b \sum_{j=1}^{k-1} (1+b)^{k-j-1} c_j + c_k \right) + c_i \quad (19)$$

We now focus only on the two sums over k and j . We shuffle the elements in the sum as follows

$$\sum_{k=1}^{i-1} \left(b \sum_{j=1}^{k-1} (1+b)^{k-j-1} c_j + c_k \right) = b \sum_{k=1}^{i-1} \sum_{j=1}^{k-1} (1+b)^{k-j-1} c_j + \sum_{k=1}^{i-1} c_k \quad (20)$$

Now, we re-order the sum so as to first sum along the j and then the k . To do this explicitly, we can introduce the variable δ_{jk} which is equal to 0 if $j \geq k$ and 1 otherwise. Then we have

$$\sum_{k=1}^{i-1} \sum_{j=1}^{k-1} (1+b)^{k-j-1} c_j = \sum_{k=1}^{i-1} \sum_{j=1}^{i-1} (1+b)^{k-j-1} c_j \delta_{jk} \quad (21)$$

$$= \sum_{j=1}^{i-1} \sum_{k=1}^{i-1} (1+b)^{k-j-1} c_j \delta_{jk} \quad (22)$$

$$= \sum_{j=1}^{i-1} \sum_{k=j+1}^{i-1} (1+b)^{k-j-1} c_j \quad (23)$$

Note that if $j = i - 1$ then $\sum_{k=j+1}^{i-1} (1+b)^{k-j-1} c_k = 0$, since the sum should start from i but the last element is $i - 1$. By re-naming the sum $\sum_{k=1}^{i-1} c_k = \sum_{j=1}^{i-1} c_j$ with respect to the variable j , we have that (20) becomes

$$b \sum_{k=1}^{i-1} \sum_{j=1}^{k-1} (1+b)^{k-j-1} c_j + \sum_{k=1}^{i-1} c_k = \sum_{j=1}^{i-1} \left(b \sum_{k=j+1}^{i-1} (1+b)^{k-j-1} c_j + c_j \right) \quad (24)$$

$$= \sum_{j=1}^{i-1} \left(b \sum_{k=j+1}^{i-1} (1+b)^{k-j-1} + 1 \right) c_j \quad (25)$$

Now, we show that

$$b \sum_{k=j+1}^{i-1} (1+b)^{k-j-1} + 1 = (1+b)^{i-j-1}. \quad (26)$$

To show this we define $\ell = k - j - 1$ and rewrite the sum as follows

$$b \sum_{k=j+1}^{i-1} (1+b)^{k-j-1} + 1 = 1 + b \sum_{\ell=0}^{i-j-2} (1+b)^\ell$$

Now, for any integer s , we prove by induction that

$$1 + b \sum_{\ell=0}^s (1+b)^\ell = (1+b)^{s+1}.$$

If $s = 0$ the statement holds. Now assume $s > 0$ and that the induction hypothesis holds for any $s' < s$. Then

$$\begin{aligned} 1 + b \sum_{\ell=0}^s (1+b)^\ell &= 1 + b \sum_{\ell=0}^{s-1} (1+b)^\ell + b(1+b)^s \\ &= (1+b)^s + b(1+b)^s \\ &= (1+b)^{s+1}, \end{aligned}$$

where we have use the inductive hypothesis for the second equality.

Applying the result above for $s = i - j - 2$ yields (26). Plugging it into (20) gives us

$$\sum_{j=1}^{i-1} \left(b \sum_{k=j+1}^{i-1} (1+b)^{k-j-1} + 1 \right) c_j = \sum_{j=1}^{i-1} (1+b)^{i-j-1} c_j \quad (27)$$

Finally, this equation can be plugged into (19) to obtain

$$a_i = \sum_{j=1}^{i-1} b(1+b)^{i-j-1} c_j + c_i,$$

concluding the proof. \square

Lemma B.4 (relaxed triangle inequality). *Let $\{\mathbf{v}_1, \dots, \mathbf{v}_n\}$ be n vectors in \mathbb{R}^d . Then, the following is true:*

$$\left\| \sum_{i=1}^n \mathbf{v}_i \right\|^2 \leq n \sum_{i=1}^n \|\mathbf{v}_i\|^2$$

Proof. By Jensen's inequality, given a convex function ϕ , a series of n vectors $\{\mathbf{v}_1, \dots, \mathbf{v}_n\}$ and a series of non-negative coefficients λ_i with $\sum_{i=1}^n \lambda_i = 1$, it results that

$$\phi \left(\sum_{i=1}^n \lambda_i \mathbf{v}_i \right) \leq \sum_{i=1}^n \lambda_i \phi(\mathbf{v}_i)$$

Since the function $\mathbf{v} \rightarrow \|\mathbf{v}\|^2$ is convex, we can use this inequality with coefficients $\lambda_1 = \dots = \lambda_n = 1/n$, with $\sum_{i=1}^n \lambda_i = 1$, and obtain that

$$\left\| \frac{1}{n} \sum_{i=1}^n \mathbf{v}_i \right\|^2 = \frac{1}{n^2} \left\| \sum_{i=1}^n \mathbf{v}_i \right\|^2 \leq \frac{1}{n} \sum_{i=1}^n \|\mathbf{v}_i\|^2$$

\square

Lemma B.5 (Geometric series with generic indexes). *Let it be $r \neq 1$ the ratio of a geometric series, b a term not constant in the summation index and constants $m \leq n$ and α , then:*

$$\sum_{k=m}^n b r^{\alpha(n-k)} = \frac{b(r^{\alpha(n-m+1)} - 1)}{r^\alpha - 1} \quad (28)$$

Proof. Apply a change of variables to the summation indexes, then use the known result, which states $\sum_{k=0}^n x^k = \frac{1-x^{n+1}}{1-x}$:

$$\begin{aligned} \sum_{k=m}^n b r^{\alpha(n-k)} &\stackrel{\tilde{r} := r^{-\alpha}}{=} \sum_{k=m}^n b \tilde{r}^{k-n} = \sum_{k=0}^{n-m} b \tilde{r}^{k-n+m} = b \tilde{r}^{m-n} \sum_{k=0}^{n-m} \tilde{r}^k \\ &= b \tilde{r}^{m-n} \left(\frac{1 - \tilde{r}^{n-m+1}}{1 - \tilde{r}} \right) = b \left(\frac{\tilde{r}^{m-n} - \tilde{r}}{1 - \tilde{r}} \right) \\ &= b \left(\frac{\tilde{r}(\tilde{r}^{m-n-1} - 1)}{\tilde{r}(\tilde{r}-1)} \right) = b \left(\frac{r^{-\alpha(m-n-1)} - 1}{r^\alpha - 1} \right) \\ &= \frac{b(r^{\alpha(n-m+1)} - 1)}{r^\alpha - 1} \end{aligned}$$

\square

Lemma B.6 (Putting a constant inside an average). *Suppose a is the average of $b_i c_i$, that is $a := \frac{1}{\sum_i^k b_i} \sum_i^k b_i c_i$, where c_i are unknown terms, i.e. cannot be expressed but with a summation. Then, for any constant d , it holds that:*

$$a + d = \frac{1}{\sum_i^k b_i} \sum_i^k b_i (c_i + d)$$

Proof. Let us rewrite $a + d$ substituting their definitions:

$$\begin{aligned} a + d &= \frac{1}{\sum_i^k b_i} \sum_i^k b_i c_i + d \frac{1}{\sum_i^k b_i} \sum_i^k b_i \\ &= \frac{1}{\sum_i^k b_i} \sum_i^k b_i c_i + \frac{1}{\sum_i^k b_i} \sum_i^k b_i d \\ &= \frac{1}{\sum_i^k b_i} \left(\sum_i^k b_i c_i + \sum_i^k b_i d \right) \\ &= \frac{1}{\sum_i^k b_i} \sum_i^k b_i (c_i + d) \end{aligned}$$

□

B.3 Proofs of main lemmas

In this section we provide the proofs of the main theoretical results presented in the main paper.

Proof of Lemma 4.5 (Deviation of τ -GHB momentum from τ -averaged gradients)

Let us start considering the left-hand side of eq. (4.5), using the notation $\alpha = 1 + \hat{\beta}$ for compactness

$$\mathbb{E} \left[\left\| \frac{\alpha - 1}{\alpha^\tau - 1} \left(\sum_{k=t-\tau}^{t-1} \alpha^{t-k-1} g^k \right) - g^{(t-1)\tau} \right\|^2 \right] = \quad (29)$$

$$\stackrel{\text{lemma B.6}}{=} \mathbb{E} \left[\left\| \frac{\alpha - 1}{\alpha^\tau - 1} \left(\sum_{k=t-\tau}^{t-1} \alpha^{t-k-1} (g^k - g^{(t-1)\tau}) \right) \right\|^2 \right] \quad (30)$$

$$= \left(\frac{\alpha - 1}{\alpha^\tau - 1} \right)^2 \sum_{k,j=t-\tau}^{t-1} \mathbb{E} \left[\left\langle \alpha^{t-k-1} (g^k - g^{(t-1)\tau}), \alpha^{t-j-1} (g^j - g^{(t-1)\tau}) \right\rangle \right] \quad (31)$$

$$\leq \left(\frac{\alpha - 1}{\alpha^\tau - 1} \right)^2 \sum_{k,j=t-\tau}^{t-1} \alpha^{2(t-1)-k-j} \left(\frac{1}{2} \mathbb{E} \left[\|g^{(t-1)\tau} - g^k\|^2 \right] + \frac{1}{2} \mathbb{E} \left[\|g^{(t-1)\tau} - g^j\|^2 \right] \right) \quad (32)$$

$$= \left(\frac{\alpha - 1}{\alpha^\tau - 1} \right)^2 \sum_{k=t-\tau}^{t-1} \left(\sum_{j=t-\tau}^{t-1} \alpha^{2(t-1)-k-j} \right) \frac{1}{2} \mathbb{E} \left[\|g^{(t-1)\tau} - g^k\|^2 \right] + \quad (33)$$

$$+ \left(\frac{\alpha - 1}{\alpha^\tau - 1} \right)^2 \sum_{j=t-\tau}^{t-1} \left(\sum_{k=t-\tau}^{t-1} \alpha^{2(t-1)-k-j} \right) \frac{1}{2} \mathbb{E} \left[\|g^{(t-1)\tau} - g^j\|^2 \right] \quad (34)$$

$$\stackrel{\text{lemma B.5}}{=} \left(\frac{\alpha - 1}{\alpha^\tau - 1} \right)^2 \sum_{k=t-\tau}^{t-1} \frac{\alpha^{t-k-1} (\alpha^\tau - 1)}{\alpha - 1} \mathbb{E} \left[\|g^{(t-1)\tau} - g^k\|^2 \right] \quad (35)$$

$$= \left(\frac{\alpha - 1}{\alpha^\tau - 1} \right) \sum_{k=t-\tau}^{t-1} \alpha^{t-k-1} \mathbb{E} \left[\|g^{(t-1)\tau} - g^k\|^2 \right] \quad (36)$$

having used the Cauchy-Schwarz inequality at (32). Now, we can manipulate and refactor the summations:

$$\left(\frac{\alpha-1}{\alpha^\tau-1}\right) \sum_{k=t-\tau}^{t-1} \alpha^{t-k-1} \mathbb{E} \left[\left\| g^{(t-1)\tau} - g^k \right\|^2 \right] = \quad (37)$$

$$= \left(\frac{\alpha-1}{\alpha^\tau-1}\right) \sum_{k=t-\tau}^{t-1} \alpha^{t-k-1} (t-k-1) \sum_{j=k}^{t-2} \mathbb{E} \left[\left\| g^{j+1} - g^j \right\|^2 \right] \quad (38)$$

$$\stackrel{\text{Assumption 4.2}}{\leq} \left(\frac{\alpha-1}{\alpha^\tau-1}\right) \sum_{k=t-\tau}^{t-1} \alpha^{t-k-1} (t-k-1) \sum_{j=k}^{t-2} L^2 \mathbb{E} \left[\left\| \theta^{j+1} - \theta^j \right\|^2 \right] \quad (39)$$

$$= \left(\frac{\alpha-1}{\alpha^\tau-1}\right) \sum_{j=t-\tau}^{t-2} \left(\sum_{k=t-\tau}^j \alpha^{t-k-1} (t-k-1) \right) L^2 \mathbb{E} \left[\left\| \theta^{j+1} - \theta^j \right\|^2 \right] \quad (40)$$

We can now exploit the fact that the term $\sum_{k=t-\tau}^j \alpha^{t-k-1} (t-k-1)$ in (40) can be bounded as

$$\sum_{k=t-\tau}^j \alpha^{t-k-1} (t-k-1) \leq (\tau-1) \sum_{k=t-\tau}^j \alpha^{t-k-1} \quad (41)$$

since the maximum of $t-k-1$ in the sum is $\tau-1$. By plugging (41) in (40), and with a refactoring, we then get:

$$\left(\frac{\alpha-1}{\alpha^\tau-1}\right) \sum_{j=t-\tau}^{t-2} \left(\sum_{k=t-\tau}^j \alpha^{t-k-1} (t-k-1) \right) L^2 \mathbb{E} \left[\left\| \theta^{j+1} - \theta^j \right\|^2 \right] \quad (42)$$

$$\leq \left(\frac{\alpha-1}{\alpha^\tau-1}\right) \sum_{j=t-\tau}^{t-2} \left((\tau-1) \alpha^{t-1} \sum_{k=t-\tau}^j \alpha^{-k} \right) L^2 \mathbb{E} \left[\left\| \theta^{j+1} - \theta^j \right\|^2 \right] \quad (43)$$

$$\stackrel{\text{lemma B.5}}{=} \left(\frac{L^2}{\alpha^\tau-1} (\tau-1)\right) \sum_{j=t-\tau}^{t-2} (\alpha^\tau - \alpha^{t-1-j}) \mathbb{E} \left[\left\| \theta^{j+1} - \theta^j \right\|^2 \right] \quad (44)$$

$$\leq \left(\frac{L^2}{\alpha^\tau-1} (\tau-1)\right) \sum_{j=t-\tau}^{t-2} (\alpha^\tau - 1) \mathbb{E} \left[\left\| \theta^{j+1} - \theta^j \right\|^2 \right] \quad (45)$$

$$= L^2 (\tau-1) \sum_{j=t-\tau}^{t-2} \mathbb{E} \left[\left\| \theta^{j+1} - \theta^j \right\|^2 \right] \quad (46)$$

where in going from (44) to (45) we used the fact that the term $\alpha^\tau - \alpha^{t-1-j}$, with $j = t-\tau, \dots, t-2$, is maximized by $\alpha^\tau - 1$ since $\alpha > 1$ and $\tau \geq 1$. This concludes the proof. \square

Proof of Lemma 4.6 (Variance of τ -GHB momentum)

Recall the definitions of drifted stochastic, un-drifted stochastic and un-drifted deterministic gradients, and let us call \tilde{m}_τ^t , \bar{m}_τ^t , m_τ^t the momentum terms built using the corresponding gradients.

We want to measure the variance of \tilde{m}_τ^t , which is measured between \tilde{m}_τ^t and its deterministic version m_τ^t . In particular, we should also keep track of the effect of multiple local steps: in fact, differently from the centralized scenario, variance of gradients due to stochastic sampling of samples is not the only source of error, since clients' gradients experience a drift. Then we have:

$$\begin{aligned} \mathbb{E} \left[\left\| \tilde{m}_\tau^t - m_\tau^t \right\|^2 \right] &= \mathbb{E} \left[\left\| \tilde{m}_\tau^t - \bar{m}_\tau^t + \bar{m}_\tau^t - m_\tau^t \right\|^2 \right] \\ &\stackrel{\text{lemma B.4}}{\leq} \underbrace{2 \mathbb{E} \left[\left\| \tilde{m}_\tau^t - \bar{m}_\tau^t \right\|^2 \right]}_{\mathcal{T}_1} + 2 \underbrace{\mathbb{E} \left[\left\| \bar{m}_\tau^t - m_\tau^t \right\|^2 \right]}_{\mathcal{T}_2} \end{aligned} \quad (47)$$

Let us consider first the term \mathcal{T}_1 in (47):

$$\mathcal{T}_1 = \mathbb{E} \left[\left\| \tilde{m}_\tau^t - \bar{m}_\tau^t \right\|^2 \right] = \mathbb{E} \left[\left\| \sum_{k=t-\tau}^{t-1} \hat{\beta}(1+\hat{\beta})^{t-k-1} \tilde{g}^k - \sum_{k=t-\tau}^{t-1} \hat{\beta}(1+\hat{\beta})^{t-k-1} \bar{g}^k \right\|^2 \right] \quad (48)$$

$$= \hat{\beta}^2 \mathbb{E} \left[\left\| \sum_{k=t-\tau}^{t-1} (1+\hat{\beta})^{t-k-1} (\tilde{g}^k - \bar{g}^k) \right\|^2 \right] \quad (49)$$

$$\stackrel{\text{lemma B.4}}{\leq} \hat{\beta}^2 \tau \sum_{k=t-\tau}^{t-1} (1+\hat{\beta})^{2(t-k-1)} \mathbb{E} \left[\left\| \tilde{g}^k - \bar{g}^k \right\|^2 \right] \quad (50)$$

$$= \frac{\beta^2}{J^2 \tau} \sum_{k=t-\tau}^{t-1} (1+\hat{\beta})^{2(t-k-1)} \mathbb{E} \left[\left\| \tilde{g}^k - \bar{g}^k \right\|^2 \right] \quad (51)$$

$$= \frac{\beta^2}{J^2 \tau} \sum_{k=t-\tau}^{t-1} (1+\hat{\beta})^{2(t-k-1)} \mathbb{E} \left[\left\| \frac{1}{|\mathcal{S}|} \sum_{i=1}^{|\mathcal{S}|} \sum_{j=1}^J \left(\tilde{g}_i^{k,j}(\theta_i^{k,j-1}) - \bar{g}_i^{k,j}(\theta_i^{k,j-1}) \right) \right\|^2 \right] \quad (52)$$

$$\stackrel{\text{lemma B.4}}{\leq} \frac{\beta^2}{J|\mathcal{S}| \tau} \sum_{k=t-\tau}^{t-1} (1+\hat{\beta})^{2(t-k-1)} \sum_{i=1}^{|\mathcal{S}|} \sum_{j=1}^J \mathbb{E} \left[\left\| \tilde{g}_i^{k,j}(\theta_i^{k,j-1}) - \bar{g}_i^{k,j}(\theta_i^{k,j-1}) \right\|^2 \right] \quad (53)$$

where in (51) and (52) we used the definition of $\hat{\beta}$ and of the gradients, respectively. Now, we can leverage the assumption of smoothness of the clients' objectives (Assumption 4.2) and the definition of client drift from equation (1), thus obtaining that:

$$\mathcal{T}_1 = \mathbb{E} \left[\left\| \tilde{m}_\tau^t - \bar{m}_\tau^t \right\|^2 \right] \leq \frac{\beta^2 L^2}{J|\mathcal{S}| \tau} \sum_{k=t-\tau}^{t-1} (1+\hat{\beta})^{2(t-k-1)} \sum_{i=1}^{|\mathcal{S}|} \sum_{j=1}^J \mathbb{E} \left[\left\| \theta_i^{k,j-1} - \bar{\theta}_i^{k,j-1} \right\|^2 \right] \quad (54)$$

$$= \frac{\beta^2 L^2}{\tau} \sum_{k=t-\tau}^{t-1} (1+\hat{\beta})^{2(t-k-1)} \epsilon_k \quad (55)$$

For ease of notation, we can now rewrite $1+\hat{\beta} := \alpha$ in (56):

$$\mathcal{T}_1 = \mathbb{E} \left[\left\| \tilde{m}_\tau^t - \bar{m}_\tau^t \right\|^2 \right] \leq \frac{\beta^2 L^2}{\tau} \sum_{k=t-\tau}^{t-1} \alpha^{2(t-k-1)} \epsilon_k \quad (56)$$

$$\leq \frac{\beta^2 L^2}{\tau} \sqrt{\sum_{k=t-\tau}^{t-1} \alpha^{4(t-k-1)}} \sqrt{\sum_{k=t-\tau}^{t-1} (\epsilon_k)^2} \quad (57)$$

$$\stackrel{\text{lemma B.5}}{=} \frac{\beta^2 L^2}{\tau} \sqrt{\frac{\alpha^{4\tau} - 1}{\alpha^4 - 1}} \sqrt{\sum_{k=t-\tau}^{t-1} (\epsilon_k)^2} \quad (58)$$

$$\stackrel{\sqrt{a+b} \leq \sqrt{a} + \sqrt{b}}{\leq} \frac{\beta^2 L^2}{\tau} \sqrt{\frac{\alpha^{4\tau} - 1}{\alpha^4 - 1}} \sum_{k=t-\tau}^{t-1} \epsilon_k \quad (59)$$

$$\stackrel{(\alpha^2 - 1)^2 \leq (\alpha^4 - 1)}{\leq} \frac{\beta^2 L^2}{\tau} \frac{\alpha^{2\tau}}{\alpha^2 - 1} \sum_{k=t-\tau}^{t-1} \epsilon_k \quad (60)$$

$$\stackrel{(\alpha - 1)^2 \leq (\alpha^2 - 1)}{\leq} \frac{\beta^2 L^2}{\tau} \frac{\alpha^{2\tau}}{(\alpha - 1)^2} \sum_{k=t-\tau}^{t-1} \epsilon_k \quad (61)$$

where we used the Cauchy-Schwarz inequality in (57).

The function $\frac{1}{\tau} \frac{\alpha^{2\tau}}{(\alpha-1)^2}$ in (61), with $\tau \geq 1$, is non-decreasing. Thus, its upper bound can be taken as:

$$\frac{1}{\tau} \frac{\alpha^{2\tau}}{(\alpha-1)^2} \leq \lim_{\tau \rightarrow \infty} \frac{1}{\tau} \frac{\alpha^{2\tau}}{(\alpha-1)^2} = \frac{e^{2\beta/J} J}{2\beta} \quad (62)$$

where we have also replaced back $\alpha := 1 + \hat{\beta}$. Thus, by plugging (62) in (61) we finally obtain that

$$\mathcal{T}_1 = \mathbb{E} \left[\|\tilde{m}_\tau^t - \bar{m}_\tau^t\|^2 \right] \leq \frac{\beta J L^2}{2} e^{2\beta/J} \sum_{k=t-\tau}^{t-1} \varepsilon_k \quad (63)$$

We can now consider the term \mathcal{T}_2 in (47). We have:

$$\mathcal{T}_2 = \mathbb{E} \left[\|\bar{m}_\tau^t - m_\tau^t\|^2 \right] = \mathbb{E} \left[\left\| \sum_{k=t-\tau}^{t-1} \hat{\beta} (1 + \hat{\beta})^{t-k-1} \bar{g}^k - \sum_{k=t-\tau}^{t-1} \hat{\beta} (1 + \hat{\beta})^{t-k-1} g^k \right\|^2 \right] \quad (64)$$

$$= \hat{\beta}^2 \mathbb{E} \left[\left\| \sum_{k=t-\tau}^{t-1} (1 + \hat{\beta})^{t-k-1} (\bar{g}^k - g^k) \right\|^2 \right] \quad (65)$$

$$\stackrel{\text{lemma B.4}}{\leq} \hat{\beta}^2 \tau \sum_{k=t-\tau}^{t-1} (1 + \hat{\beta})^{2(t-k-1)} \mathbb{E} \left[\|\bar{g}^k - g^k\|^2 \right] \quad (66)$$

$$= \frac{\beta^2}{J^2 \tau} \sum_{k=t-\tau}^{t-1} (1 + \hat{\beta})^{2(t-k-1)} \mathbb{E} \left[\|\bar{g}^k - g^k\|^2 \right] \quad (67)$$

$$= \frac{\beta^2}{J^2 \tau} \sum_{k=t-\tau}^{t-1} (1 + \hat{\beta})^{2(t-k-1)} \mathbb{E} \left[\left\| \frac{1}{|\mathcal{S}|} \sum_{i=1}^{|\mathcal{S}|} \sum_{j=1}^J (\tilde{g}_i^{k,j}(\theta^{k,j-1}) - g_i^{k,j}(\theta^{k,j-1})) \right\|^2 \right] \quad (68)$$

$$\stackrel{\text{lemma B.4}}{\leq} \frac{\beta^2}{J |\mathcal{S}| \tau} \sum_{k=t-\tau}^{t-1} (1 + \hat{\beta})^{2(t-k-1)} \sum_{i=1}^{|\mathcal{S}|} \sum_{j=1}^J \mathbb{E} \left[\left\| \tilde{g}_i^{k,j}(\theta^{k,j-1}) - g_i^{k,j}(\theta^{k,j-1}) \right\|^2 \right] \quad (69)$$

where in (67) and (68) we used the definition of $\hat{\beta}$ and of the gradients, respectively. Now, we can leverage Assumption 4.1, thus obtaining that:

$$\mathcal{T}_2 = \mathbb{E} \left[\|\bar{m}_\tau^t - m_\tau^t\|^2 \right] \leq \frac{\beta^2}{\tau} \sum_{k=t-\tau}^{t-1} (1 + \hat{\beta})^{2(t-k-1)} \sigma^2 \quad (70)$$

$$\stackrel{\alpha := (1 + \hat{\beta})}{=} \frac{\beta^2}{\tau} \sum_{k=t-\tau}^{t-1} \alpha^{2(t-k-1)} \sigma^2 \quad (71)$$

$$\stackrel{\text{lemma B.5}}{=} \frac{\beta^2 \sigma^2}{\tau} \frac{\alpha^{2\tau} - 1}{\alpha^2 - 1} \quad (72)$$

The function $\frac{1}{\tau} \frac{\alpha^{2\tau} - 1}{\alpha^2 - 1}$ in (72), with $\tau \geq 1$, is non-decreasing. Thus, its upper bound can be taken as:

$$\frac{1}{\tau} \frac{\alpha^{2\tau} - 1}{\alpha^2 - 1} \leq \lim_{\tau \rightarrow \infty} \frac{1}{\tau} \frac{\alpha^{2\tau} - 1}{\alpha^2 - 1} = \frac{-1 + e^{2\beta/J} J}{2\beta} \quad (73)$$

where we have also replaced back $\alpha := 1 + \hat{\beta}$. Thus, by plugging (73) in (72) we finally obtain that

$$\mathcal{T}_2 = \mathbb{E} \left[\|\tilde{m}_\tau^t - m_\tau^t\|^2 \right] \leq \frac{\beta J}{2} (-1 + e^{2\beta/J}) \sigma^2 \leq \frac{\beta J}{2} e^{2\beta/J} \sigma^2 \quad (74)$$

Having found upper bounds (63) for \mathcal{T}_1 and (74) for \mathcal{T}_2 , we can plug them in (47), thus obtaining that

$$\mathbb{E} \left[\|\tilde{m}_\tau^t - m_\tau^t\|^2 \right] \leq 2\mathcal{T}_1 + 2\mathcal{T}_2 \leq \beta J e^{2\beta/J} \left(L^2 \sum_{k=t-\tau}^{t-1} \varepsilon_k + \sigma^2 \right) \quad (75)$$

which concludes the proof. \square

Proof of Lemma 4.7 (Deviation of τ -averaged gradient from true gradient)

Let define $\mathcal{S}_d := \mathcal{S} - \mathcal{S}_\tau^t$ and $\mathcal{S}_i := \mathcal{S} \cap \mathcal{S}_\tau^t$. With this, we can expand the terms at the left-hand side using their definitions as follows:

$$\mathbb{E} \left[\|g^{t_\tau} - g^t\|^2 \right] = \mathbb{E} \left[\left\| \frac{1}{|\mathcal{S}_\tau^t|} \sum_{i=1}^{|\mathcal{S}_\tau^t|} g_i^t - \frac{1}{|\mathcal{S}|} \sum_{i=1}^{|\mathcal{S}|} g_i^t \right\|^2 \right] \quad (76)$$

$$= \mathbb{E} \left[\left\| \sum_{i \in \mathcal{S}_i} \left(\frac{1}{|\mathcal{S}_\tau^t|} - \frac{1}{|\mathcal{S}|} \right) g_i^t - \sum_{k \in \mathcal{S}_d} \frac{1}{|\mathcal{S}|} g_k^t \right\|^2 \right] \quad (77)$$

$$\stackrel{\text{lemma B.4}}{\leq} 2 \left(\underbrace{\mathbb{E} \left[\left\| \sum_{i \in \mathcal{S}_i} \left(\frac{1}{|\mathcal{S}_\tau^t|} - \frac{1}{|\mathcal{S}|} \right) g_i^t \right\|^2 \right]}_{\mathcal{T}_3} + \underbrace{\mathbb{E} \left[\left\| \sum_{k \in \mathcal{S}_d} \frac{1}{|\mathcal{S}|} g_k^t \right\|^2 \right]}_{\mathcal{T}_4} \right) \quad (78)$$

$$(79)$$

Let us consider first \mathcal{T}_3 . We have:

$$\mathcal{T}_3 = \mathbb{E} \left[\left\| \sum_{i \in \mathcal{S}_i} \left(\frac{1}{|\mathcal{S}_\tau^t|} - \frac{1}{|\mathcal{S}|} \right) g_i^t \right\|^2 \right] = \mathbb{E} \left[\left(\frac{1}{|\mathcal{S}_\tau^t|} - \frac{1}{|\mathcal{S}|} \right)^2 \left\| \sum_{i \in \mathcal{S}_i} g_i^t \right\|^2 \right] \quad (80)$$

$$\stackrel{\text{lemma B.4}}{\leq} \mathbb{E} \left[\left(\frac{1}{|\mathcal{S}_\tau^t|} - \frac{1}{|\mathcal{S}|} \right)^2 |\mathcal{S}_i| \sum_{i \in \mathcal{S}_i} \|g_i^t\|^2 \right] \quad (81)$$

$$= \mathbb{E} \left[\left(\frac{1}{|\mathcal{S}_\tau^t|} - \frac{1}{|\mathcal{S}|} \right)^2 |\mathcal{S}_i| \sum_{i \in \mathcal{S}_i} \|g_i^t - g^t + g^t\|^2 \right] \quad (82)$$

$$\stackrel{\text{lemma B.4}}{\leq} 2 \mathbb{E} \left[\left(\frac{1}{|\mathcal{S}_\tau^t|} - \frac{1}{|\mathcal{S}|} \right)^2 |\mathcal{S}_i| \sum_{i \in \mathcal{S}_i} (\|g_i^t - g^t\|^2 + \|g^t\|^2) \right] \quad (83)$$

$$\stackrel{\text{assumption 4.3}}{\leq} 2 \mathbb{E} \left[\left(\frac{1}{|\mathcal{S}_\tau^t|} - \frac{1}{|\mathcal{S}|} \right)^2 |\mathcal{S}_i| \left(|\mathcal{S}_i| G^2 + \sum_{i \in \mathcal{S}_i} \|g^t\|^2 \right) \right] \quad (84)$$

Since the term g^t does not depend on the index i , we get

$$2\mathbb{E} \left[\left(\frac{1}{|\mathcal{S}_\tau^t|} - \frac{1}{|\mathcal{S}|} \right)^2 |\mathcal{S}_i| \left(|\mathcal{S}_i| G^2 + \sum_{i \in \mathcal{S}_i} \|g^t\|^2 \right) \right] = 2\mathbb{E} \left[\left(\frac{1}{|\mathcal{S}_\tau^t|} - \frac{1}{|\mathcal{S}|} \right)^2 |\mathcal{S}_i| \left(|\mathcal{S}_i| G^2 + |\mathcal{S}_i| \|g^t\|^2 \right) \right] \quad (85)$$

$$= 2\mathbb{E} \left[\left(\frac{1}{|\mathcal{S}_\tau^t|} - \frac{1}{|\mathcal{S}|} \right)^2 |\mathcal{S}_i|^2 \right] (G^2 + \|g^t\|^2) \quad (86)$$

Now, note that $\mathcal{S}_\tau^t \subseteq \mathcal{S} \implies |\mathcal{S}_i| = |\mathcal{S}_\tau^t|$. Therefore,

$$\mathcal{T}_3 \leq 2\mathbb{E} \left[\left(\frac{1}{|\mathcal{S}_\tau^t|} - \frac{1}{|\mathcal{S}|} \right)^2 |\mathcal{S}_i|^2 \right] (G^2 + \|g^t\|^2) = 2\mathbb{E} \left[\left(\frac{|\mathcal{S}| - |\mathcal{S}_\tau^t|}{|\mathcal{S}|} \right)^2 \right] (G^2 + \|g^t\|^2) \quad (87)$$

Moving now to \mathcal{T}_4 , we have:

$$\mathcal{T}_4 = \mathbb{E} \left[\left\| \sum_{k \in \mathcal{S}_d} \frac{1}{|\mathcal{S}|} g_k^t \right\|^2 \right] \leq \mathbb{E} \left[\left(\frac{1}{|\mathcal{S}|} \right)^2 \left\| \sum_{k \in \mathcal{S}_d} g_k^t \right\|^2 \right] \quad (88)$$

$$\stackrel{\text{lemma B.4}}{\leq} \mathbb{E} \left[\left(\frac{1}{|\mathcal{S}|} \right)^2 |\mathcal{S}_d| \sum_{k \in \mathcal{S}_d} \|g_k^t\|^2 \right] \quad (89)$$

$$= \mathbb{E} \left[\left(\frac{1}{|\mathcal{S}|} \right)^2 |\mathcal{S}_d| \sum_{k \in \mathcal{S}_d} \|g_k^t - g^t + g^t\|^2 \right] \quad (90)$$

$$\stackrel{\text{lemma B.4}}{\leq} 2\mathbb{E} \left[\left(\frac{1}{|\mathcal{S}|} \right)^2 |\mathcal{S}_d| \sum_{k \in \mathcal{S}_d} (\|g_k^t - g^t\|^2 + \|g^t\|^2) \right] \quad (91)$$

$$\stackrel{\text{assumption 4.3}}{\leq} 2\mathbb{E} \left[\left(\frac{1}{|\mathcal{S}|} \right)^2 |\mathcal{S}_d| \left(|\mathcal{S}_d| G^2 + \sum_{k \in \mathcal{S}_d} \|g^t\|^2 \right) \right] \quad (92)$$

$$= 2\mathbb{E} \left[\left(\frac{1}{|\mathcal{S}|} \right)^2 |\mathcal{S}_d| \left(|\mathcal{S}_d| G^2 + |\mathcal{S}_d| \|g^t\|^2 \right) \right] \quad (93)$$

$$= 2\mathbb{E} \left[\left(\frac{|\mathcal{S}_d|}{|\mathcal{S}|} \right)^2 \right] (G^2 + \|g^t\|^2) \quad (94)$$

$$(95)$$

Observing that $|\mathcal{S}_d| = |\mathcal{S}| - |\mathcal{S}_\tau^t|$ we obtain:

$$\mathcal{T}_4 \leq 2\mathbb{E} \left[\left(\frac{|\mathcal{S}_d|}{|\mathcal{S}|} \right)^2 \right] (G^2 + \|g^t\|^2) = \mathbb{E} \left[\left(\frac{|\mathcal{S}| - |\mathcal{S}_\tau^t|}{|\mathcal{S}|} \right)^2 \right] (G^2 + \|g^t\|^2) \quad (96)$$

Finally, by plugging (87) and (96) in (78) we obtain

$$\mathbb{E}_{\mathcal{S}^t \sim \mathcal{U}(\mathcal{S})} \left[\left\| g^{(t)\tau}(\theta) - g^t(\theta) \right\|^2 \right] \leq 8\mathbb{E}_{\mathcal{S}^t \sim \mathcal{U}(\mathcal{S})} \left[\left(\frac{|\mathcal{S}| - |\mathcal{S}_\tau^t|}{|\mathcal{S}|} \right)^2 \right] (G^2 + \|g^t\|^2)$$

which concludes the proof. \square

Proof of Corollary 4.8 This corollary follows from Lemma 4.7, which states that

$$\mathbb{E}_{\mathcal{S}^t \sim \mathcal{U}(\mathcal{S})} \left[\left\| g^{(t)\tau}(\theta) - g^t(\theta) \right\|^2 \right] \leq 8 \mathbb{E}_{\mathcal{S}^t \sim \mathcal{U}(\mathcal{S})} \left[\left(\frac{|\mathcal{S}| - |\mathcal{S}_\tau^t|}{|\mathcal{S}|} \right)^2 \right] \left(G^2 + \|g^t\|^2 \right)$$

To prove the results, we use (i) assumption 4.4, (ii) the fact that $|\mathcal{S}^t| = |\mathcal{S}|C \forall t$ and (iii) \mathcal{S}_τ^t is union of τ disjoint \mathcal{S}^t sets. Using points (i)-(iii), and assuming $\tau \in [0, \frac{1}{C}]$, it follows that:

$$\left\| g^{(t)\tau}(\theta) - g^t(\theta) \right\|^2 \leq 8(1 - \tau C)^2 \left(G^2 + \|g^t\|^2 \right)$$

C Experimental Results

C.1 Datasets and Models

CIFAR-10/100 We consider CIFAR-10 and CIFAR-100 to experiment with image classification tasks, each one respectively having 10 and 100 classes. For all methods, training images are pre-processed by applying random crops, followed by random horizontal flips. Both training and test images are finally normalized according to their mean and standard deviation. As the main model for experimentation, we used a model similar to LeNet-5 as proposed in [14]. To further validate our findings, we also employed a ResNet-20 as described in [11], following the implementation provided in [15]. Since batch normalization [16] layers have been shown to hamper performance in learning from decentralized data with skewed label distribution [12], we replaced them with group normalization [39], using two groups in each layer. For a fair comparison, we used the same modified network also in centralized training. We report the result of centralized training for reference in Table 4: as per the hyperparameters, we use 64 for the batch size, 0.01 and 0.1 for the learning rate respectively for the LeNet and the ResNet-20 and 0.9 for momentum. We trained both models on both datasets for 150 epochs using a cosine annealing learning rate scheduler.

Shakespeare The Shakespeare language modeling dataset is created by collating the collective works of William Shakespeare and originally comprises 715 clients, with each client denoting a speaking role. However, for this study, a different approach was used, adopting the LEAF [5] framework to split the dataset among 100 devices and restrict the number of data points per device to 2000. The non-IID dataset is formed by assigning each device to a specific role, and the local dataset for each device contains the sentences from that role. Conversely, the IID dataset is created by randomly distributing sentences from all roles across the devices.

Table 4: Test accuracy (%) of centralized training over datasets and models used. Results are reported in term of mean top-1 accuracy over the last 10 epochs, averaged over 5 independent runs.

DATASET	ACC. CENTRALIZED (%)
CIFAR-10 w/ LEnET	86.48 ± 0.22
CIFAR-10 w/ RESNET-20	89.05 ± 0.44
CIFAR-100 w/ LEnET	57.00 ± 0.09
CIFAR-100 w/ RESNET-20	62.21 ± 0.85
SHAKESPEARE	52.00 ± 0.16
STACKOVERFLOW	28.50 ± 0.25
GLDV2	74.03 ± 0.15

For this task, we have employed a two-layer Long Short-Term Memory (LSTM) classifier, consisting of 100 hidden units and an 8-dimensional embedding layer. Our objective is to predict the next character in a sequence, where there are a total of 80 possible character classes. The model takes in a sequence of 80 characters as input, and for each character, it learns an 8-dimensional representation. The final output of the model is a single character prediction for each training example, achieved through the use of 2 LSTM layers and a densely-connected layer followed by a softmax. This model architecture is the same used by [24, 1].

We report the result of centralized training for reference in Table 4: we train for 75 epochs with constant learning rate, using as hyperparameters 100 for the batch size, 1 for the learning rate, 0.0001 for the weight decay and no momentum.

StackOverflow The Stack Overflow dataset is a language modeling corpus that comprises questions and answers from the popular Q&A website, StackOverflow. Initially, the dataset consists of 342477 unique users but for, practical reasons, we limit our analysis to a subset of 40k users. Our goal is to perform the next-word prediction on these text sequences. To achieve this, we utilize a Recurrent Neural Network (RNN) that first learns a 96-dimensional representation for each word in a sentence and then processes them through a single LSTM layer with a hidden dimension of 670. Finally, the

model generates predictions using a densely connected softmax output layer. The model and the preprocessing steps are the same as in [30].

We report the result of centralized training for reference in Table 4: as per the hyperparameters, we use 16 for the batch size, $10^{-1/2}$ for the learning rate and no momentum or weight decay. We train for 50 epochs with a constant learning rate.

Given the size of the test dataset, testing on STACKOVERFLOW is conducted on a subset of them made by 10000 randomly chosen test examples, selected at the beginning of training.

Large-scale real-world datasets As large-scale real-world datasets for our experimentation, we follow [14]. GLDV2 is composed of $\approx 164k$ images belonging to ≈ 2000 classes, realistically split among 1262 clients. INATURALIST is composed of $\approx 120k$ images belonging to ≈ 1200 classes, split among 9275 clients. These datasets are challenging to train not only because of their inherent complexity (size of images, number of classes) but also because usually at each round a very small portion of clients is selected. In particular, for GLDV2 we sample 10 clients per round, while for INATURALIST we experiment with different participation rates, sampling 10, 50, or 100 clients per round. In the main paper, we choose to report the participation rate instead of the number of sampled clients to better highlight that the tested scenarios are closer to a cross-device setting, which is the most challenging for algorithms based on client participation, like SCAFFOLD and ours. As per the model, for both datasets, we use a MobileNetV2 pretrained on ImageNet.

Table 5: Details about datasets’ split used for our experiments

	CIFAR-10	CIFAR-100	SHAKESPEARE	STACKOVERFLOW	GLDV2	INATURALIST
Clients	100	100	100	40.000	1262	9275
Number of clients per round	10	10	10	50	10	{10, 50, 100}
Number of classes	10	100	80	10004	2028	1203
Avg. examples per client	500	500	2000	428	130	13
Number of local steps	8	8	20	27	13	2
Average participation (round no.)	1k	1k	25	1.5	40	{5, 27, 54}

C.2 Simulating heterogeneity

For CIFAR-10/100 we simulate arbitrary heterogeneity by splitting the total datasets according to a Dirichlet distribution with concentration parameter α , following [14]. In practice, we draw a multinomial $q_i \sim \text{Dir}(\alpha p)$ from a Dirichlet distribution, where p describes a prior class distribution over N classes, and α controls the heterogeneity among all clients: the greater α the more homogeneous the clients’ data distributions will be. After drawing the class distributions q_i , for every client i , we sample training examples for each class according to q_i without replacement.

In the main paper, we considered only two levels of heterogeneity: the first uses $\alpha = 0$ and is used to simulate a pathological non-iid scenario, while the second uses $\alpha = 10k$ and corresponds to having homogeneous local datasets. To further investigate the impact of heterogeneity, we provide the results for different values of α in section C.6 of this supplementary.

C.3 Evaluating communication and computational cost

In the main paper we showed a comparison in communication and computational cost of state-of-art FL algorithms compared to our solutions GHBM and FEDHBM: in this section we detail how those results in table Tab. 3 have been obtained. We follow a three-step procedure:

1. For each algorithm a , we calculate the minimum number of rounds r_a to reach the performance of FEDAVG, the total amount of bytes exchanged b_a in the whole training budget (number of rounds, as described in Appendix C.5) and the measure the corresponding total training time t_a . In this way, the different requirements in communication and computation of each algorithm are taken into account for the next steps.
2. We calculate the actual communication and computational requirements as $(tb_a = b_a \cdot s_a, tt_a = t_a \cdot s_a)$, where $s_a = \frac{r_a}{T}$ is the speedup of the algorithm w.r.t. FEDAVG. For those competitor algorithms that did not reach the target performance (*e.g.* MIMEMOM) in the training budget T , we conservatively consider $r_a = T$. In this way, the convergence speed of each algorithm is taken into account for determining the actual amount of computation needed.

3. We complement the above information with with a reduction/increase factor w.r.t. FEDAVG, calculated as $rtb_a = \left(1 - \frac{tb_a}{tb_{\text{FEDAVG}}}\right)$ and $rta_a = \left(1 - \frac{ta_a}{ta_{\text{FEDAVG}}}\right)$ and expressed as a percentage. A cost reduction (*i.e.* $rtb_a > 0$ or $rta_a > 0$) is indicated with \downarrow , while a cost increase (*i.e.* $rtb_a < 0$ or $rta_a < 0$) is indicated with \uparrow . This gives a practical indication of how much communication/computation have been saved in choosing the algorithm at hand as an alternative for FEDAVG.

C.4 Hyperparameters

For ease of consultation, we report the hyper-parameters grids as well as the chosen values in Table 6. For GLDV2 and INATURALIST we only test the best SOTA algorithms: FEDAVG and FEDAVGM as baselines, SCAFFOLD and MIMEMOM.

MOBILENETV2 For all algorithms we perform $E = 5$ local epochs, and searched $\eta \in \{0.1, 1\}$ and $\eta_l \in \{0.01, 0.1\}$, and found $\eta = 0.1, \eta_l = 0.1$ works best for FEDAVGM, while $\eta = 1, \eta_l = 0.1$ works best for the others. For INATURALIST, we had to enlarge the grid for SCAFFOLD and MIMEMOM: for both we searched $\eta \in \{10^{-3/2}, 10^{-1}, 10^{-1/2}, 1\}$ and $\eta_l \in \{10^{-2}, 10^{-3/2}, 10^{-1}, 10^{-1/2}\}$.

VIT-B16 For all algorithms we perform $E = 5$ local epochs, and searched $\eta \in \{0.1, 1\}$ and $\eta_l \in \{0.03, 0.01\}$ following [34], and found $\eta = 0.1, \eta_l = 0.03$ works best for FEDAVGM, while $\eta = 1, \eta_l = 0.03$ works best for the others.

Table 6: Hyper-parameter search grid for each combination of method and dataset (for $\alpha = 0$). The best values are indicated in **bold**.

METHOD	HPARAM	CIFAR-10/100		SHAKESPEARE	STACKOVERFLOW
		LENET	RESNET-20		
ALL FL	wd B	[0.001 , 0.0008, 0.0004] 64	[0.0001, 0.00001] 64	[0, 0.0001, 0.00001] 100	[0, 0.0001, 0.00001] 16
FEDAVG	η η_l	[1, 0.5, 0.1] [0.1, 0.05, 0.01]	[1, 0.1] [0.1 , 0.01]	[1, 0.5, 0.1] [1, 0.5, 0.1]	[1, 0.5, 0.1] [1, 0.5, 0.3 , 0.1]
FEDPROX	η η_l μ	[1, 0.5, 0.1] [0.1, 0.05, 0.01] [0.1 , 0.01, 0.001]	[1, 0.1] [0.1 , 0.01] [0.1 , 0.01, 0.001]	[1, 0.5, 0.1] [1, 0.5, 0.1] [0.1, 0.01, 0.001, 0.0001]	[1, 0.5, 0.1] [1, 0.5, 0.3 , 0.1] [0.1, 0.01 , 0.001, 0.0001]
SCAFFOLD	η η_l	[1, 0.5, 0.1] [0.1, 0.05, 0.01]	[1, 0.1] [0.1 , 0.01]	[1, 0.5, 0.1] [1, 0.5, 0.1]	[1, 0.5, 0.1] [1, 0.5, 0.3 , 0.1]
FEDDYN	η η_l α	[1, 0.5, 0.1] [0.1, 0.05, 0.01] [0.1, 0.01, 0.001]	[1, 0.1] [0.1, 0.01] [0.1, 0.01, 0.001]	[1, 0.5, 0.1] [1, 0.5, 0.1] [0.1, 0.009 , 0.001]	[1, 0.5, 0.1] [1, 0.5, 0.3 , 0.1] [0.1 , 0.009, 0.001]
ADABEST	η η_l α	[1, 0.5, 0.1] [0.1, 0.05, 0.01] [0.1, 0.01, 0.001]	[1, 0.5, 0.1] [0.1, 0.05, 0.01] [0.1, 0.01, 0.001]	[1, 0.5, 0.1] [1, 0.5, 0.1] [0.1, 0.009 , 0.001]	[1, 0.5, 0.1] [1, 0.5, 0.3 , 0.1] [0.1 , 0.009, 0.001]
MIME	η η_l	[1, 0.5, 0.1] [0.1, 0.05, 0.01]	[1, 0.1] [0.1, 0.01]	[1, 0.5, 0.1] [1, 0.5, 0.1]	[1, 0.5, 0.1] [1, 0.5, 0.3 , 0.1]
FEDAVGM	η η_l β	[1, 0.5, 0.1] [0.1, 0.05, 0.01] [0.99, 0.9]	[1, 0.1] [0.1 , 0.01] [0.99, 0.9]	[1, 0.5, 0.1] [1, 0.5, 0.1] [0.99, 0.9]	[1, 0.5, 0.1] [1, 0.5, 0.3 , 0.1] [0.99, 0.9]
MIMEMOM	η η_l β	[1, 0.5, 0.1] [0.1, 0.05, 0.01] [0.99, 0.95, 0.9]	[1, 0.5, 0.3, 0.1] [0.1 , 0.05, 0.03, 0.01] [0.99, 0.95, 0.9]	[1, 0.5, 0.1] [1, 0.5, 0.1] [0.99, 0.9]	[1, 0.5, 0.1] [1, 0.5, 0.3, 0.1] [0.99, 0.9]
MIMELITEMOM	η η_l β	[1, 0.5, 0.1] [0.1, 0.05, 0.01] [0.99, 0.9]	[1, 0.5, 0.3, 0.1] [0.1 , 0.05, 0.03, 0.01] [0.99, 0.95, 0.9]	[1, 0.5, 0.1] [1, 0.5, 0.1] [0.99, 0.9]	[1, 0.5, 0.1] [1, 0.5, 0.3, 0.1] [0.99, 0.9]
FEDCM	η η_l α	[1, 0.5, 0.1] [1, 0.5, 0.1] [0.05, 0.1 , 0.5]	[1, 0.5, 0.1] [1, 0.5, 0.1] [0.05, 0.1 , 0.5]	[1, 0.5, 0.1] [1, 0.5, 0.1] [0.05, 0.1 , 0.5]	- - -
GHBM (ours)	η η_l β τ	[1, 0.5, 0.1] [1, 0.5, 0.1] [0.9] [5, 10 , 20, 40]	[1, 0.1] [1, 0.5, 0.1] [0.9] [5, 10 , 20, 40]	[1, 0.5, 0.1] [1, 0.5, 0.1] [0.9] [5, 10 , 20, 40]	[1, 0.5, 0.1] [1, 0.5, 0.3 , 0.1] [0.9] [5, 10 , 20, 40]
FEDHBM(ours)	η η_l β	[1, 0.5, 0.1] [0.1, 0.05, 0.01] [1, 0.99, 0.9]	[1, 0.1] [0.1, 0.01] [1, 0.99, 0.9]	[1, 0.5, 0.1] [1, 0.5, 0.1] [1, 0.99, 0.9]	[1, 0.5, 0.1] [1, 0.5, 0.3 , 0.1] [1, 0.99, 0.9]

C.5 Implementation details

We implemented all the tested algorithms and training procedures in a single codebase, using PYTORCH 1.10 framework, compiled with CUDA 10.2. The federated learning setup is simulated by using a single node equipped with 11 Intel(R) Core(TM) i7-6850K CPUs and 4 NVIDIA GeForce GTX 1070 GPUs. For the large-scale experiments we used the computing capabilities offered by LEONARDO cluster of CINECA-HPC, employing nodes equipped with 1 CPU Intel(R) Xeon 8358 32 core, 2,6 GHz CPUs and 4 NVIDIA A100 SXM6 64GB (VRAM) GPUs. The simulation always runs in a sequential manner (on a single GPU) the parallel client training and the following aggregation by the central server.

Practicality of experiments Under the above conditions, a single FEDAVG experiment on CIFAR-100 takes $\approx 02:05$ hours (CNN, with $T = 20.000$) and $\approx 03:36$ hours (RESNET-20, with $T = 10.000$). For SCAFFOLD we always use the "option II" of their algorithm [18] to calculate the client controls, incurring almost no overhead in our simulations. We found that using "option I" usually degrades both final model quality and requires almost the double the training time, due to the additional forward+backward passes. Conversely, all MIME's methods incur a significant overhead due to the additional round needed to calculate the full-batch gradients, taking $\approx 10:40$ hours for CIFAR-100 with RESNET-20. On SHAKESPEARE and STACKOVERFLOW, FEDAVG takes ≈ 22 minutes and ≈ 3.5 hours to run respectively $T = 250$ and $T = 1500$ rounds.

C.6 Additional Experiments

Experiments on CIFAR-10 Table 7 reports the results of experiments analogous to the ones presented in Tab. 1. For the main paper, we report experiments on CIFAR-100, as it is a more complex dataset and often a more reliable testing ground for FL algorithms. Indeed, sometimes algorithms perform well on CIFAR-10 but worse on CIFAR-100 (as for the already discussed case of FEDDYN). Results in Tab. 7 confirm the findings of the main paper: under extreme heterogeneity, some algorithms behave inconsistently across CNN and RESNET-20 (notice that FEDDYN and MIMELITEMOM only with CNN improve FEDAVG. Conversely, LOCAL-GHBM and FEDHBM both consistently improve the state-of-art by a large margin.

Table 7: Test accuracy (%) comparison of SOTA FL algorithms in a controlled setting. Best result is in **bold**, second best is underlined.

METHOD	CIFAR-10 (RESNET-20)		CIFAR-10 (CNN)	
	NON-IID	IID	NON-IID	IID
FEDAVG	61.0 \pm 1.0	86.4 \pm 0.2	66.1 \pm 0.3	83.1 \pm 0.3
FEDPROX	61.0 \pm 1.8	86.7 \pm 0.2	66.1 \pm 0.3	83.1 \pm 0.3
SCAFFOLD	71.8 \pm 1.7	86.8 \pm 0.3	74.8 \pm 0.2	82.9 \pm 0.2
FEDDYN	60.2 \pm 3.0	87.0 \pm 0.3	70.9 \pm 0.2	83.5 \pm 0.1
ADABEST	73.6 \pm 3.0	86.7 \pm 0.5	66.1 \pm 0.3	83.1 \pm 0.4
MIME	53.7 \pm 2.9	86.7 \pm 0.1	75.1 \pm 0.5	83.1 \pm 0.2
FEDAVGM	66.0 \pm 2.2	87.7 \pm 0.3	67.6 \pm 0.3	83.6 \pm 0.3
FEDCM(GHBM $\tau=1$)	65.2 \pm 3.2	87.1 \pm 0.3	69.0 \pm 0.3	83.4 \pm 0.3
FEDADC(GHBM $\tau=1$)	65.7 \pm 3.0	87.1 \pm 0.2	66.1 \pm 0.3	83.4 \pm 0.3
MIMEMOM	69.2 \pm 3.6	88.0 \pm 0.1	80.9 \pm 0.4	83.1 \pm 0.2
MIMELITEMOM	57.0 \pm 0.9	88.0 \pm 0.4	78.8 \pm 0.4	83.2 \pm 0.3
LOCAL-GHBM (ours)	<u>80.6 \pm 0.3</u>	<u>88.8 \pm 0.1</u>	<u>81.1 \pm 0.3</u>	<u>83.7 \pm 0.1</u>
FEDHBM (ours)	83.4 \pm 0.3	89.2 \pm 0.1	81.7 \pm 0.1	83.8 \pm 0.1

Effect of different levels of heterogeneity Figure 4 presents an analysis of the effect of heterogeneity on (i) final model quality (left) and (ii) convergence speed (right). The experimental results, while confirming that it is crucial to perform some form of drift control during local optimization, show that momentum methods handle extreme heterogeneity scenarios better than methods that rely on stochastic variance reduction, such as SCAFFOLD. Let us notice that the considered algorithms are robust w.r.t. non-extreme heterogeneity: this underlines the need for algorithms that do not sacrifice communication efficiency for robustness to heterogeneity. The right part of the figure shows that heterogeneity has a strong effect also on convergence speed. In line with the results on the left graph, MIMEMOM and FEDHBM are the fastest when facing the pathological case of $\alpha = 0$. Surprisingly, MIMEMOM is not significantly faster than FEDAVG and FEDAVGM in non-extremely heterogeneous scenarios; indeed it is slower if taking into account the communication overhead. In all cases FEDHBM performs best, demonstrating high robustness to heterogeneity from both the considered perspectives.

Leveraging pre-trained models In Sec. 3.4 we showed that under the very low participation rates experienced on GLDV2 and INATURALIST, the first time each client is selected we can calculate the momentum client side by leveraging the pretrained model.

In this section we better discuss the motivation behind this choice, and provide additional evidence in controlled settings. From line 6 of Algorithm 1, in settings akin to cross-device FL most of the time

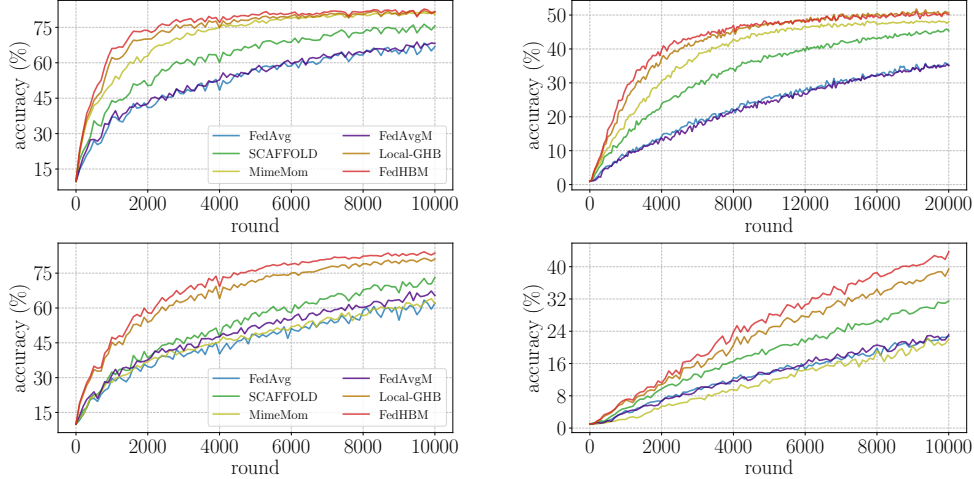
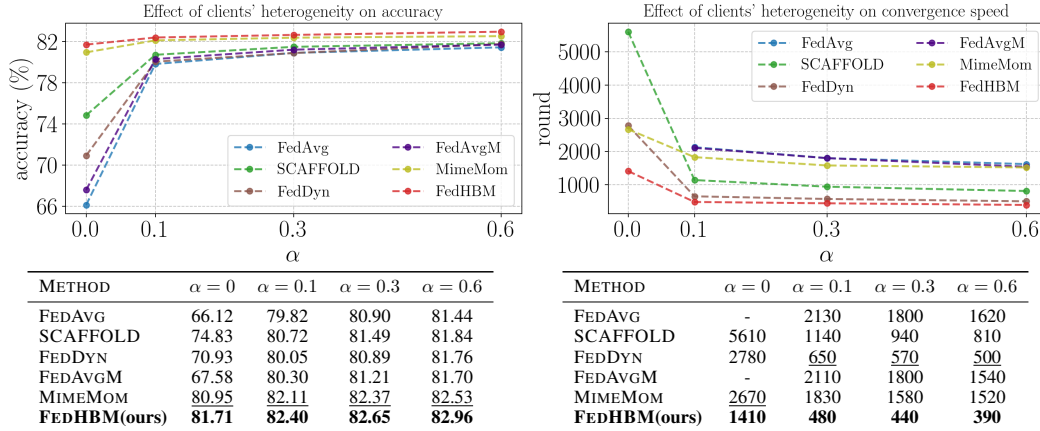


Figure 3: Accuracy plot of the best performing algorithms on CIFAR-10 (left, Tab. 7) and CIFAR-100 (right, Tab. 1) on CNN (top) and RESNET-20 (bottom), on our most heterogeneous setting ($\alpha = 0$).

Figure 4: Ablation study on the effect of several degrees of heterogeneity on performance of SOTA algorithms and FEDHBM on CIFAR-10 and CNN. The left figure shows the final accuracy reached by algorithms, while the right figure shows the number of rounds needed to reach 70% of absolute accuracy. The tables show the values depicted in the respective picture above. The best results are in **bold**, second best are in underlined.



the momentum term will be equal to zero, as only when clients get selected for the second time it will be possible to calculate the momentum term. While in those settings it may be more appropriate to use GHBM and treat τ as a hyperparameter, in this work we tried to investigate whether FEDHBM is still a good and practical choice.

A practical idea to overcome the above limitation is considering the starting model θ^0 as past model. In such a way, it is possible to enjoy the corrective effect of momentum without waiting for each client to be selected at least once. Let us note that this does not require additional communication: when training a model from scratch, it is necessary to know only the initialization algorithm and the seed for the random number generator to recover the very same model client side. However, for practical cases in which this information is unknown or it is desirable to keep it private, we also experiment letting each client use a different random initialization. These two variations are referred in Fig. 5a as FEDHBM-shared and FEDHBM-random. As it possible to notice, they are quite robust and allow recovering prompt acceleration in settings with critically low participation, like in the STACKOVERFLOW case, where each client each client is selected 1.5 times on average during the whole training.

This technique can be used also when the training does not start from scratch, but from a pretrained model, without compromising communication efficiency. In fact, the pretrained model can be asynchronously downloaded from a server different than the FL training orchestrator. We experiment by letting the initial server model have the feature extractor initialized from a pre-trained model (on CIFAR-100 for CIFAR-10 and vice versa). As illustrated in Fig. 5b and 5c, this modification allows regaining full speed from early rounds of training, thereby demonstrating the efficacy of leveraging a well-initialized model for prompt acceleration.

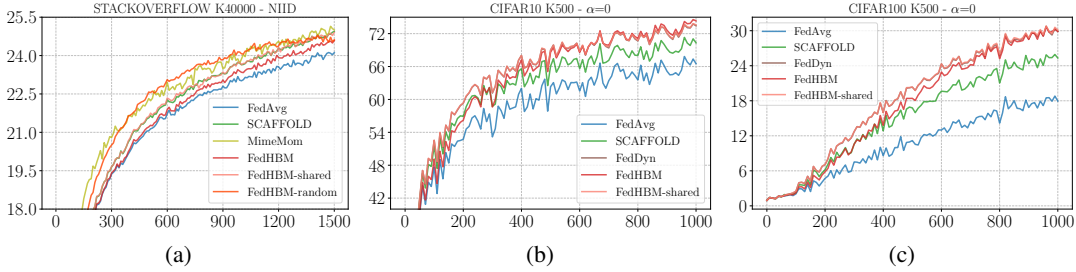


Figure 5: Effect of using a shared model as initialization. For CIFAR’s we show the impact of using a pre-trained backbone, while for STACKOVERFLOW we analyze the use of a random shared or independent model initialization.

C.7 About the use of learning rate schedulers

For simplicity, in all our FL experiments we did not use any learning rate scheduler. In fact, while using strategies to change the learning rate as training proceeds is in general beneficial, this would result in a difficult tuning of hyper-parameters associated with the scheduler, since the algorithms present very different convergence rates.

Let us also point out that many well-established works in FL do not use learning rate schedules [26, 24, 13, 18, 19], while some others do [1]. Figure 6 shows the accuracy curves of the best FL algorithms from Tab. 1, using a learning rate decay with decay coefficient fine-tuned for each algorithm, searched in the range $\{0.999, 0.9992, 0.9995, 0.9999\}$. For all the algorithms, the best learning rate decay turned out to be 0.9999. Comparing with performances without learning rate decay, it is possible to notice that: (i) the use of learning rate decay, in general, does not change the relative performance of the algorithms; (ii) in these settings, the use of learning rate decay does not help convergence. This is particularly true in non-iid scenario, where the performances are degraded w.r.t. not applying any schedule. This is motivated by the fact that a large number of rounds is needed to achieve convergence, and probably the simple decay strategy adopted from [1] is not optimal to practically give an advantage. Other learning rate schedules may be more appropriate, but this largely expands the needed hyperparameter search, considering that it must be searched separately for each algorithm.

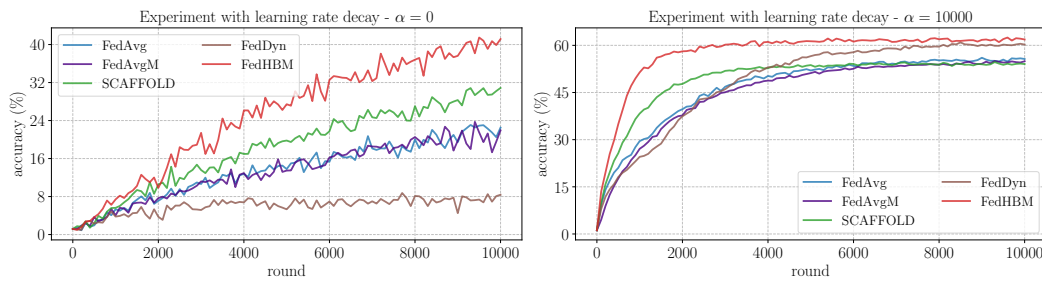


Figure 6: Experiments with learning rate decay of SOTA algorithms and FEDHBM on CIFAR-100 with RESNET-20. The decay coefficient has been searched in the range $\{0.999, 0.9992, 0.9995, 0.9999\}$ separately for each algorithm.